ELSEVIER

Coordination Chemistry Reviews
199 (2000) 1–53

COORDINATION CHEMISTRY REVIEWS

www.elsevier.com/locate/ccr

Pressure-tuning spectroscopy of inorganic compounds: a summary of the past 15 years

Clare M. Edwards, Ian S. Butler *

Department of Chemistry, McGill University, 801 Sherbrooke Street West, Montreal, Que., Canada, H3A 2K6

Received 1 September 1998; accepted 30 April 1999

Contents

Abstract

Since its development over 40 years ago, the diamond–anvil cell has been widely used to study the high-pressure behavior of numerous materials and compounds. Pressures from a

* Corresponding author.

PII: S0010-8545(99)00150-2

few kbar to a Mbar can easily be achieved and the transparent diamonds provide an optical window for in-situ measurements. Pressure-tuning spectroscopy allows researchers to examine the effect of decreased inter- and intramolecular and atomic distances and the resultant orbital perturbations. This review summarizes some interesting results of pressure-tuning infrared, Raman and electronic spectroscopic studies for a variety of inter- and intramolecular interactions including metal–CO π-backbonding, metal–metal interactions in dimers, clusters, and one-dimensional compounds, order–disorder transitions of CH_3 and NH_3 ligands and hydrogen bonding.

Keywords: Diamond–anvil cell; Pressure-tuning; Vibrational spectroscopy; Electronic spectroscopy; Phase transitions

1. Introduction

Compared to temperature, pressure is a much less explored physical variable. The diamond–anvil cell (DAC) is probably the most widely known high-pressure device for scientific studies. Although the DAC offers only a tiny sample volume, the simplicity of its design, the range of attainable pressures, and the wide variety of experiments possible make the DAC very attractive for the study of all kinds of materials under compression. After nearly 40 years since its development by Alvin Van Valkenburg and Charles Weir, then at the National Bureau of Standards in Washington DC [1], the DAC has found its way into many areas of research and scientific analysis ranging from physics and chemistry to geology, biochemistry, and forensic science. Diamond–anvil cells, capable of achieving pressures of the order of 500 kbar to 1 Mbar, have allowed geologists to determine the high-pressure structures of minerals and to relate geophysical phenomena to pressure-induced phase transitions in minerals [2]. In materials science, the use of more modest pressures, up to 200 kbar, has afforded insight into structure–property relationships of solids, for example, of magnetic materials, and in the pressure-tuning of the band-gaps in semiconductor materials [3]. More recently, high hydrostatic pressures produced in DACs have led to the synthesis of new compounds, e.g. the solid state polymerization of acetylene in solution at 42 kbar [4], and the synthesis of sp^2-bonded carbon nitrides [5].

Compression of a material results in a decrease in sample volume, a decrease in inter- and intramolecular and atomic distances and so an increase in orbital overlap. The perturbation of the orbitals will depend on the types of orbital involved. Pressure-tuning studies of the vibrational and electronic levels of a material permit an examination of its optical, electrical, magnetic and chemical properties.

In 1984, Ferraro published his classic book entitled 'Vibrational Spectroscopy at High External Pressures: The Diamond–Anvil Cell' [6], in which he describes the effect of high, external pressures on a wide variety of inorganic, coordination, and organic and biological compounds. Since then, a number of concise reviews have appeared, notably by Drickamer [7], who has focused his attention on pressure-tun-

ing electronic spectroscopy. The construction and techniques associated with high-pressure devices have also been reviewed, e.g. see Refs. [8,9].

The present review is directed towards a summary of pressure-tuning IR, Raman and electronic spectroscopic studies of selected coordination and organometallic compounds, which have afforded some particularly interesting results. The review is by no means exhaustive, but offers an overview of the work done is this area over the past 15 years, since Ferraro's book. Many coordination compounds have been studied by high-pressure X-ray diffraction techniques as well as by other methods, but these results are not included here. In addition this review does not attempt to describe fully the practical aspects of using DACs or the theory associated with pressure-induced shifts in vibrational and electronic spectra. A brief description, with some references, of the practicalities of using DACs, along with a qualitative introduction to the theory, is given in the first section, in order to provide an basis for the discussion of the results in later sections.

2. The diamond–anvil cell

The opposed-anvil, lever-arm design of a DAC consists of two polished diamonds with flat faces, between which the sample is placed in a gasket. Pressure is applied by simply turning a screw which forces the diamond–anvils together. There are several commercially available DACs. One of the most commonly used is that built by High-pressure Diamond Optics, Tuscon, Arizona. The P-II type DAC is suitable for pressure-tuning Raman and FT-IR measurements up to ~ 70 kbar. Fig. 1 shows a schematic of the design of the cell. The diamond anvils are mounted on hardened steel and held in alignment in a cylinder as pressure is applied. The Super pressure cell can achieve much higher pressures, up to 700 kbar; its design is based on a piston–cylinder arrangement, with the diamond–anvils mounted on tungsten carbide mounts.

In the DAC, the diamonds act as both the pressure bearing medium and as the optical window. The transparency of diamonds over the whole range of the electromagnetic spectrum, except vacuum UV, allows the study of materials directly in the DAC at high, static pressures, not only through visual techniques and refractive index measurements, but by scattering techniques, e.g. X-ray diffraction, Brilloiun scattering, and by various spectroscopies including IR absorption and reflection, fluorescence and Raman. For FT-IR and FT-Raman work, the selection of the diamonds is particularly important. In the case of IR, the purest diamonds with no nitrogen impurities, type IIa, are preferred. Unfortunately, these diamonds have a tendency to cleave easily and so do not always make the best high-pressure anvils. The strongest anvils seem to contain a reasonable amount of evenly dispersed, nitrogen platelet impurity, type I, but this impurity causes considerable absorption in the mid-IR region. Even type IIa diamonds absorb in the mid-IR, in the 2400–1900 cm^{-1} region, as shown in Fig. 2. Cell designs, which use just one diamond anvil, and/or 180° scattering geometry [10], can minimize the amount of absorption. For Raman studies, the diamond anvils are often screened for low

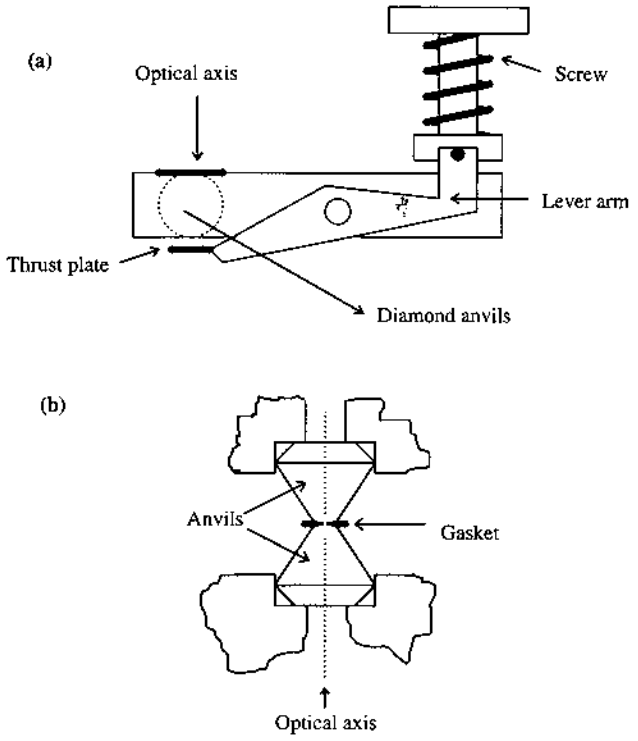

Fig. 1. Schematic of the diamond–anvil cell from high pressure diamond optics. (a) Side view. (b) The diamond–anvils and gasket.

fluorescence. Type IIb diamonds, the most expensive, have been shown to be better in some cases, but generally it is more a case of luck! Another high-pressure window material that has been examined is sapphire. Compared to type II diamonds, sapphire windows show much less fluorescence over a range of laser excitation lines [10a]. However, the use of sapphire anvils is limited to a maximum pressure of ~ 12 kbar. Gem-cut single crystal cubic zirconia anvils have recently been investigated for high-pressure optical cells [11]. A maximum pressure of 132 kbar was achieved, which was dependent on the pressure transmitting medium and the gasket material employed. Background florescence and Raman scattering from the anvils was eliminated and IR spectra could be recorded between 4000 and 1500 cm^{-1} without interference. A further example of a method to improve the intensity of the signal from diamond–anvil cells has involved the use of a microlens placed next to the outer face of the diamond–anvil. Light beams, that would have normally been lost in the wall of the support, are now focused out of the DAC. The gain in the Raman intensity appeared to be more than a factor of 3, but the background, mainly due to florescence from the diamond, increased by just 20% [12].

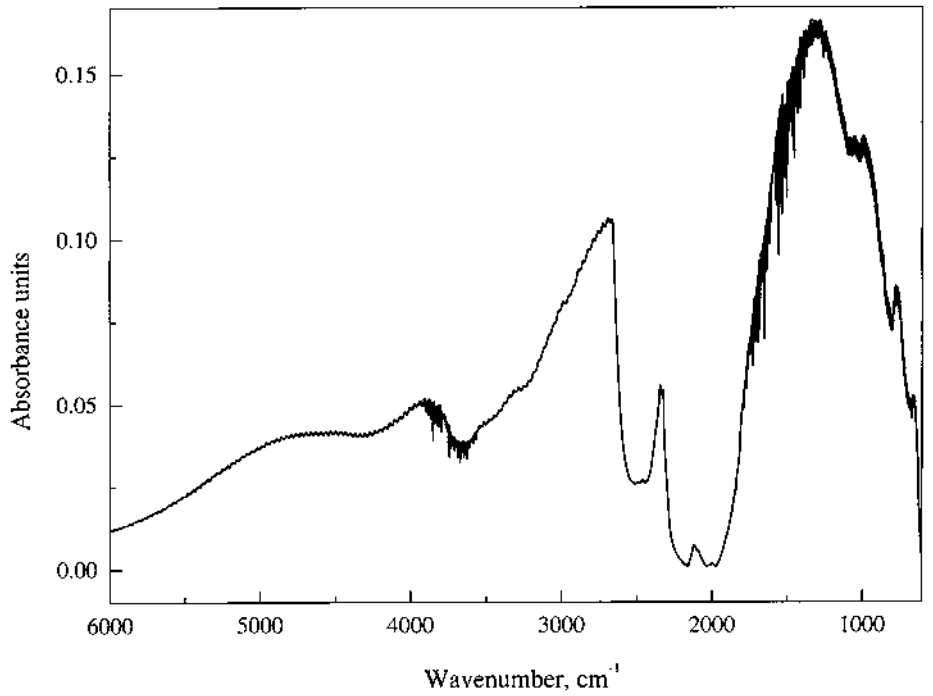

Fig. 2. Mid-IR absorption spectrum of type IIa diamond–anvils in a DAC, showing the strong absorption band in the 2400–1900 cm^{-1} region.

The introduction of gaskets has permitted the study of single crystals and fluids, since it has provided a sample chamber. The gasket also creates more hydrostatic conditions, minimizing pressure gradients across the sample area [13]. Gaskets, made from stainless steel, rhenium or inconel, for example, are often pre-indented before drilling the central sample hole. The thickness of the gasket and the size of the drilled hole will determine, in part, the maximum pressure that can be achieved. As DACs are pushed to reach ever increasing pressures, the culet face of the diamond anvil becomes smaller and so does the gasket hole. For instance, diamond anvils with 50-μm faces are required for multi-megabar experiments, requiring gasket hole diameters as small as 25-μm. As gasket holes become smaller, the task of drilling the hole becomes more difficult and time consuming, and as a result, new drilling methods are also explored, see, for example, Ref. [14].

In most high-pressure devices, the pressures are generated in the uni-axial sense, and pressure transmitting media are required to translate the pressure into a stress that is distributed uniformly. Pressure-transmitting media are especially important for experiments above 100 kbar, where significant pressure gradients can develop. Pressure-transmitting media can be gases, fluids or solids. They need to be chemically inert, have zero penetration into the sample or construction materials, have zero compressibility and be easy to handle and contained within the high-pres-

sure enclosure. Gases are the most difficult to work with since more excessive technical design of the high-pressure device is required. They are, however, advantageous because of there low viscosity. Fluids are the most practical choice for pressure-transmitting media in the DAC. Pure, single component liquids tend to crystallize at relatively modest pressures, whereas a mixture of liquids can be taken to pressures well above the freezing pressure of the individual components. Under compression, the viscosity of such mixtures tends to rise exponentially, eventually forming a glass. The viscosity of the mixture is important—if too low, the sample will flow in the DAC during analysis while, if too large, other problems can arise. A damp mixture of ethanol and methanol in a 4:1 ratio is one of the most common pressure-transmitting media used. At room temperature, the glass transition point is ~ 104 kbar, but in some cases the viscosity can become very large by ~ 70 kbar. Other fluids used in the DAC are Nujol and silicones. The choice of pressure-transmitting medium will often depend on the pressure range being investigated. For example, silicone fluid can be used to create hydrostatic conditions up to 150 kbar, after which broadening of the R_1 fluorescence line of the ruby calibrant (see below) has been reported, probably as a result of distributions in stresses [15]. Above 225 kbar, the R_1 and R_2 ruby fluorescence peaks are difficult to distinguish as they are broadened and overlap.

3. Calibration

The need for a secondary pressure gauge in the determination of the internal pressures in DACs and other high-pressure devices became evident when it was realized that the usual way in which pressure was determined, i.e. force-over-area, became unreliable at high pressures. High pressures are considered to be those above 1 kbar (1000 atm). Ideally, the pressure gauge must show a fairly linear response of some property under high static pressures, and not require a large sample volume, since the sample chamber of the DAC is obviously very small already. The precision of the gauge depends on both the precision with which the physical property can be measured and the rate at which this property changes under compression.

One of the first reliable methods of pressure calibration in the 100–300 kbar range was an X-ray pressure gauge. NaCl is a high symmetry solid, which shows a continuous volume change under compression up to its phase transition to the CsCl structure at 294 kbar. The lattice spacing of NaCl can be used to the determine the pressure by making use of the Decker equation of state for NaCl [16].

For pressure-tuning vibrational spectroscopy, an optical pressure gauge is obviously more convenient and perhaps the most well known is the ruby fluorescence R_1 line. At ambient pressures, the R_1 and R_2 ruby fluorescence lines lie at 694.1 and 692.6 nm, respectively. A continuous calibration of the ruby R_1 fluorescence gauge from 0.06 to 1 Mbar has been made, and the generally accepted equation for the pressure dependence is $P\ (\text{Mbar}) = (19.04/5)\{[(\lambda_o + \Delta\lambda)/\lambda_o]^5 - 1\}$, where λ_o is the wavelength measured at 1 bar [17]. Pressure differences or strain in the DAC can be

monitored by looking at the ruby R_1–R_2 doublet, which will broaden at high pressures as a result of pressure gradients and/or strain.

The ruby fluorescence gauge is suitable for measurements with a visible laser system. For pressure-tuning FT-Raman spectroscopy, however, the NIR Nd^{3+}:YAG laser at 1064.1 nm is too far removed to excite the ruby fluorescence and hence two Raman measurements would be required. For this reason, the development of a new secondary pressure gauge for use in FT-Raman measurements was needed. A second drawback to the pressure-tuning FT-Raman spectroscopic technique is the need for a high-sample loading. Therefore, the possibility of using the 1332.5 cm^{-1} Raman active t_{2g} phonon band of the diamond windows in the DAC was investigated as a potential in-situ pressure calibrant. This method obviously does not require the addition of material to the sample chamber and so a maximum loading of sample is still possible. The Raman-active diamond line has been shown to have a linear response to pressure over the 50–200 kbar range [18], and several mathematical models have been proposed to relate the effects of the pressure dependence of the normal modes of vibration of solids to the pressure shift of the diamond line [19]. The shift of the Raman-active t_{2g} phonon line of the diamond, as a possible internal calibrant for FT-Raman studies, has recently been investigated [20]. Under compression, the stress in the diamond–anvil is concentrated in the region near the sample–diamond interface, for the 0.001 to $\sim$70 kbar range. As pressure discontinuities in the diamond–anvil form perpendicular to the pressure axis, the diamond band at the sample–diamond interface shifts with a linear response with increasing pressure [21]. Since Raman scatter is collected in a 180° geometry from the DAC, scattering from all depths of the diamond–anvil contributes to the diamond line and a band envelope is observed. It is the wavenumber of the band half-front which is measured to determine the pressure (Fig. 3) [22]. The rate of the shift of the t_{2g} phone appears to be specific for each DAC.

For pressure-tuning IR spectroscopy, the frequency shift of the antisymmetric N–O stretching bands of dilute solutions of sodium nitrite and sodium nitrate ions in sodium bromide are used to calculate the internal pressure [23]. The band positions at ambient pressure are 1279.0 and 1403.1 cm^{-1}, respectively. The pressure is related to the shift, Δv (cm^{-1}), of the wavenumber of the nitrite ion from zero pressure by p (kbar) $= 2.356(\Delta v) - [1.334(\Delta v)\exp(\Delta v/92)]$ and to the shift, Δv (cm^{-1}), of the frequency of the nitrate ion by p (kbar) $= 1.775(\Delta v) - [0.7495(\Delta v)\exp(\Delta v/78)]$.

4. Theory

4.1. Effect of pressure on the vibrations in solids

High-pressure infrared and Raman experiments involve the monitoring of the effects, at a molecular level, of changes in the intra- and intermolecular distances

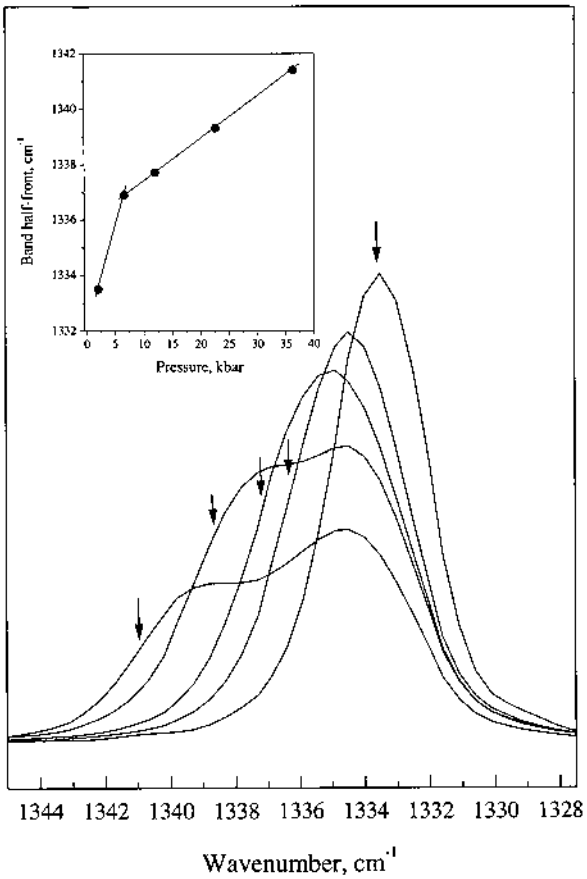

Fig. 3. FT-Raman (Nd^{3+}:YAG) spectrum of the Raman-active t_{2g} phonon mode of the diamond anvil. The arrows indicate the band half-front used to calculate the applied pressure (inset).

that are produced by pressure. The most noticeable effect is pressure-induced frequency shifts. In a completely harmonic approximation, where the force constant operating between two masses is truly a constant and independent of the distance between the masses, the application of pressure would cause no observed frequency shift at all. Therefore, the study of pressure-induced frequency shifts can be considered to be the study of the anharmonicity of atomic and/or molecular interactions.

The frequency, bandshape and intensity of a normal mode of vibration is governed by the masses of the moving nuclei, the magnitudes of the restoring forces as they are displaced along the normal coordinate, the distortion of the electron clouds that accompany the nuclear displacement, and the anharmonic coupling to other vibrational modes. Under compression, the equilibrium spacing between the nuclei changes, which distorts the electron cloud and the restoring forces, while the

nuclear masses are not affected. Isotopic substitution experiments, in which the mass changes but everything else remains unaltered, are the complement to the pressure experiment.

The frequency shifts caused by the application of modest, hydrostatic pressures do not usually significantly affect the form of the normal coordinate. As the form of the vibration is not changed and the mass remains the same, then it is only the force constant change that causes the frequency shift. Many studies focus on the change in effective force constant that comes from the change in internuclear spacing coupled with the anharmonic nature of interatomic, and inter- and intramolecular interactions. It has been shown that, for both internal and external modes of vibration, the pressure-induced frequency shifts follow directly from the anharmonicity of the bonds coupled with the changes in internuclear spacing caused by the pressure.

Theory has shown [24] that weak interactions are more anharmonic than are strong chemical bonds. However, even the strongest bond, whether in small molecules or in hard crystals, still show an anharmonicity of about -6% per 1% change in spacing. The initial rate of change for a Lennard-Jones type potential function is -21% for a 1% change in spacing. The range of frequency shifts with pressure is 1–3 cm^{-1} $kbar^{-1}$ for external modes. For internal bond stretching modes, the shifts are 0.3–1 cm^{-1} $kbar^{-1}$. Bond-bending modes are less affected and pressure shifts are of the order of 0.1–0.3 cm^{-1} $kbar^{-1}$. Any deviations from these values usually arise because of the particular nature of the interactions, e.g. π-backbonding interactions in organometallic complexes, or intra- and intermolecular interactions, such as hydrogen bonding.

4.2. Effect of pressure on electronic transitions

The initial effect of compression is to stabilize a bonding orbital relative to its antibonding combination, for a given molecular bond. For a transition from the bonding to the antibonding orbital, the energy of the transition increases (blue shift) as the pressure increases. However, in this simple model, the intermolecular interactions experienced by the molecules in the crystal lattice or in solution are not taken into account. The primary intermolecular interaction, for larger molecular ions, is an attractive van der Waals force, which can be expressed as:

$$E \sim -(\alpha_1\alpha_2/R^6)$$

where R is the distance between the interacting species, α_1 is the polarizability of the molecule or bond, and α_2 is the polarizability of the medium as seen by the electron cloud of the molecule. In general, although not always, the molecule is more polarizable when the electron is in the antibonding orbital since it is less tightly bound when in the excited state. The contribution of the intermolecular interaction to the pressure shift of an electronic transition is a red-shift, i.e. to lower energy. Many of the examples of pressure-tuning electronic absorption spectroscopy reveal the different degrees of balance between the intramolecular and intermolecular forces [7e].

4.3. Phase transitions

It is particularly interesting when the application of pressure induces a phase transition from one crystalline form to another. Phase transitions can be first-order or second-order in nature. The Gibbs free energy, G, is defined for a given mass of material by $G = U - TS + PV$. For two phases to be in thermodynamic equilibrium at a particular pressure and temperature, the Gibbs free energy must be the same for the material in either phase. A transition is referred to as first-order if the first derivative of the free energy is discontinuous at the phase change, e.g. if there is a volume discontinuity, then this indicates a first-order transition because $V = (\delta G/\delta P)_T$. However, if there is no discontinuity in the first derivative of G, but there is a discontinuity in the second derivative, then the transition is termed second-order or continuous. Thus, if the volume changes continuously, but the compressibility shows a discontinuity, then this is a second-order transition and $K = -(1/V)(\delta V/\delta P)_T = -(1/V)(\delta^2 G/\delta^2 P)$. Plots of frequency versus pressure reveal discontinuities in the slope of the graph at the pressure where a phase transition occurs. Group theory is often considered in the identification of a phase transition. Changes in molecular or crystal structure will be evident from close inspection of the number of IR and/or Raman bands and comparison with group theory.

Vibrational soft modes are often associated with a phase transition. A soft mode is a vibrational mode, the frequency of which goes to zero as the temperature or pressure approaches the phase transition temperature or pressure, respectively. Structural phase transitions are generally accompanied by crystal distortions or displacements of ions and molecules, the mean value of such a displacement corresponding to an order parameter.

4.4. Bandshapes and intensities as a function of pressure

There is no single straightforward hypothesis which can be used to treat intensity and bandshape changes as a function of pressure in the way that the frequencies were treated in terms of bond anharmonicities. For a given vibration, that is both IR and Raman active, its frequency and frequency shift with pressure will be the same. However, the band shape can be quite different and change in a different way with response to pressure. Intensities in the Raman and IR are often complementary, but both may increase, decrease, or change in opposite senses on the application of pressure. In most cases, any bandshape or intensity changes observed are small. Any significant changes are generally associated with a phase change, Fermi resonance, soft modes, hindered rotations, or, uni-axial pressure, for example.

5. Effect of pressure on vibrational and electronic spectra

5.1. Metal–carbonyls and other complexes with π-backbonding ligands

Transition metal–carbonyl complexes have attracted considerable attention for many years as they are used as catalysts in many reaction processes. The bonding

between a metal and carbonyl ligand has dual character. A metal←carbonyl σ-bond is formed by using an unshared pair of electrons on the carbon (Fig. 4a) and the formation of a metal→carbon π-bond results from donation of electrons from a filled metal orbital of suitable symmetry into the π-antibonding orbital of the carbonyl ligand (Fig. 4b). The bonding is synergic, which means that as the extent of σ-donation increases, this will tend to promote an increase in the π-backbonding, as the amount of electron density at the metal center becomes too high. The extent of σ-donation and π-backbonding can be monitored in metal carbonyl complexes by measuring the frequencies of the ν(CO) and ν(M–CO) stretching modes.

Adams and Ekejiuba first reported the effect of applied pressure on metal-carbonyl interactions in 1982 [25]. They were looking at the high-pressure Raman spectra of $Mn(CO)_5Br$ up to 50 kbar, as part of a broad study of the phase behavior of inorganic molecular crystals. Changes in the slopes of the wavenumber versus pressure plots were observed at 24 ± 3 kbar, but the lack of any discontinuity at this pressure and the ease of reversibility, suggested a second-order transition. All the internal and lattice modes showed a positive pressure dependence with the exception of ν_2, the a_1, axial ν(CO) mode, which exhibited a small negative pressure shift from ambient pressure to 23 kbar of -0.067 cm^{-1} kbar^{-1}. Above 23 kbar, the pressure dependence became positive, 0.239 cm^{-1} kbar^{-1}. The other ν(CO) modes showed continuous, but small, positive pressure dependences over the pressure range studied. Adams and Ekejiuba were the first to propose an increase in π-backbonding to the CO ligand under compression, as a result of the lower force constant of the M–CO bond compared to that of the C–O bond. As a consequence, a negative shift of the frequency of the ν(CO) modes is observed. However, lattice compression tends to raise the energies of all modes. The small, negative pressure shift of the axial ν(CO) mode in $Mn(CO)_5Br$ suggests that the increase in π-backbonding with pressure is proportionally greater for the axial CO than is that for the equatorial CO ligands.

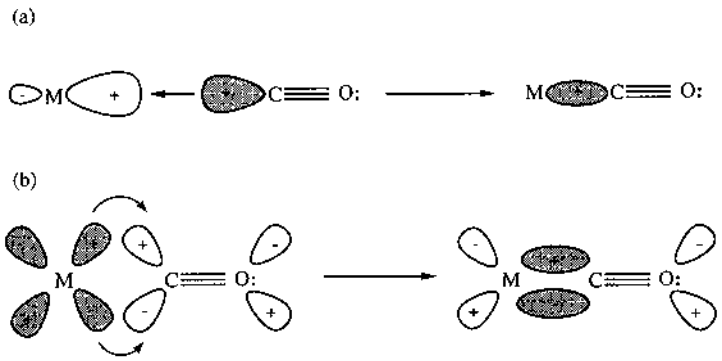

Fig. 4. (a) The formation of the metal←carbon σ-bond using an unshared pair of electrons on the carbon atom. (b) The formation of the metal→carbon π-bond.

Very similar behavior has been found for other pentacarbonyl–halide and pentacarbonyl–methyl complexes, almost all of which are isomorphous with $Mn(CO)_5Br$. The micro-Raman spectra of pentacarbonyl(chloro)rhenium(I), $Re(CO)_5Cl$, from ambient pressure to ~ 60 kbar, showed discontinuities in several bands, including ν(CO), in the wavenumber versus pressure plots [26]. These discontinuities were accounted for by a second-order phase transition, as was observed for $Mn(CO)_5Br$. For $Re(CO)_5Cl$, it was shown that the a_1^{eq} ν(CO) mode shifts steadily towards higher energies with increasing pressures and is insensitive to the phase transition. The a_1^{ax} ν(CO) mode, on the other hand, has a small, negative $d\nu/dp$ value in the low-pressure phase of -0.011 cm^{-1} kbar^{-1}. As a result of the decreasing intramolecular separations, it is normal to observe increased factor group splitting. From a factor group analysis, the b_1 ν(CO) mode would be expected to split into a doublet ($a_g = b_{2g}$). This is indeed the case for the b_1 ν(CO) mode of $CH_3Re(CO)_5$ [27]. The reverse is true for $Re(CO)_5Cl$, however, with the doublet quickly collapsing into a singlet at ~ 5 kbar, indicating that relatively strong intermolecular vibrational coupling is in fact lifted upon the application of pressure.

In contrast, neither $Re(CO)_5Br$ nor $Re(CO)_5I$ undergo a phase change under compression to 43 kbar [28]. The latter crystallizes in a different space group (*Cmcm*) from its isostructural congeners (*Pnma*) due to a different mode of packing, linked presumably to the increase in halogen size from the bromide to iodide. All the modes showed a hardening (increase in wavenumbers) with the increase of pressure. Furthermore, for $Re(CO)_5I$, the a_1, ν_6, ν(Re–I) and e, ν_{20}, δ(C–Re–C) modes, initially at 163 and 128 cm^{-1}, respectively, show a crossover point near 30 kbar. Since this is only possible if the modes are of different symmetry, assignment of these modes was confirmed. The effect of pressure on the vibrational modes of $Re(CO)_5Cl$, $Mn(CO)_5Br$, $Re(CO)_5Br$ and $Re(CO)_5I$ is summarized in Table 1.

The micro-Raman spectra of $CH_3Re(CO)_5$ and $CH_3Mn(CO)_5$ have been studied under pressures up to 40 kbar [27]. The vibrational data showed discontinuities in the wavenumber versus pressure plots at ~ 9 kbar for $CH_3Mn(CO)_5$ and 22 kbar for $CH_3Re(CO)_5$ (Fig. 5). No phase transitions were detected in a previous low-temperature vibrational study [29] and since the discontinuities were not abrupt, the pressure-induced phase transitions are likely to be second-order. The pressure dependences of the ν(CO) modes revealed a similar pattern to those seen for the pentacarbonyl halides, but the pressure dependences of the modes increased upon replacing an electron-withdrawing halide ligand with an electron-donating methyl ligand. Prior to the phase transition, the application of pressure caused a preferential increase in the extent of π-backbonding to the axial CO ligand, but to different extents for the Mn and Re complexes. At higher pressures, the effect of pressure on the π-backbonding was different for $CH_3Mn(CO)_5$ and $CH_3Re(CO)_5$. The $\nu(CO^{eq})$ modes exhibited a positive shift with an increase in pressure for both complexes. For $CH_3Mn(CO)_5$, the $\nu(CO^{ax})$ mode showed a negative pressure dependence up to 9 kbar of -0.82 cm^{-1} kbar^{-1}. Following the phase transition, the pressure dependence became positive, 0.3 cm^{-1} kbar^{-1}. The $\nu(CO^{ax})$ mode of

Table 1
Wavenumber ν (cm^{-1}) for the Raman-active ν(CO) modes and the ν(M–X) mode in $M(CO)_5X$, (M = Re, Mn; X = Cl, Br, I) and their pressure dependence, $d\nu/dp$ (cm^{-1} $kbar^{-1}$)

$Re(CO)_5Cl$[c]				$Mn(CO)_5Br$[d]				$Re(CO)_5Br$[e]		$Re(CO)_5I$[e]		Assignment
Low-pressure phase		High-pressure phase		Low-pressure phase		High-pressure phase						
ν	$d\nu/dp$	ν	$d\nu/dp$	ν	$d\nu/dp$	ν	$d\nu/dp$	ν	$d\nu/dp$	ν	$d\nu/dp$	
2157	0.38	[a]	–	2139	0.139	a	–	2156	0.30	2150	0.43	$\nu(CO^{eq})$, a_1
2090	0.36	[a]	–	2088	0.328	a	–	2088	0.30	–	–	ν(CO), b_1
2073	0.16	2078	0.31	2074	0.171	a	–	2073	0.17	2074	0.28	ν(CO), e
2031	0.11	2035	0.22									$''$
1960	−0.01	1961	0.15	1988	−0.067		0.239	1964	0.11	1984	0	$\nu(CO^{ax})$, a_1
1954	−0.01	[b]	–									
1926	−0.11	[b]	–									$\nu(^{12}CO^{ax})$, a_1
289	1.15	[b]	–	218	0.702	–	0.239	218	0.20	163	0.34	ν(M–X)

[a] Slope unchanged after phase transition.
[b] Peak too weak to measure.
[c] Ref. [26].
[d] Ref. [25].
[e] Ref. [28].

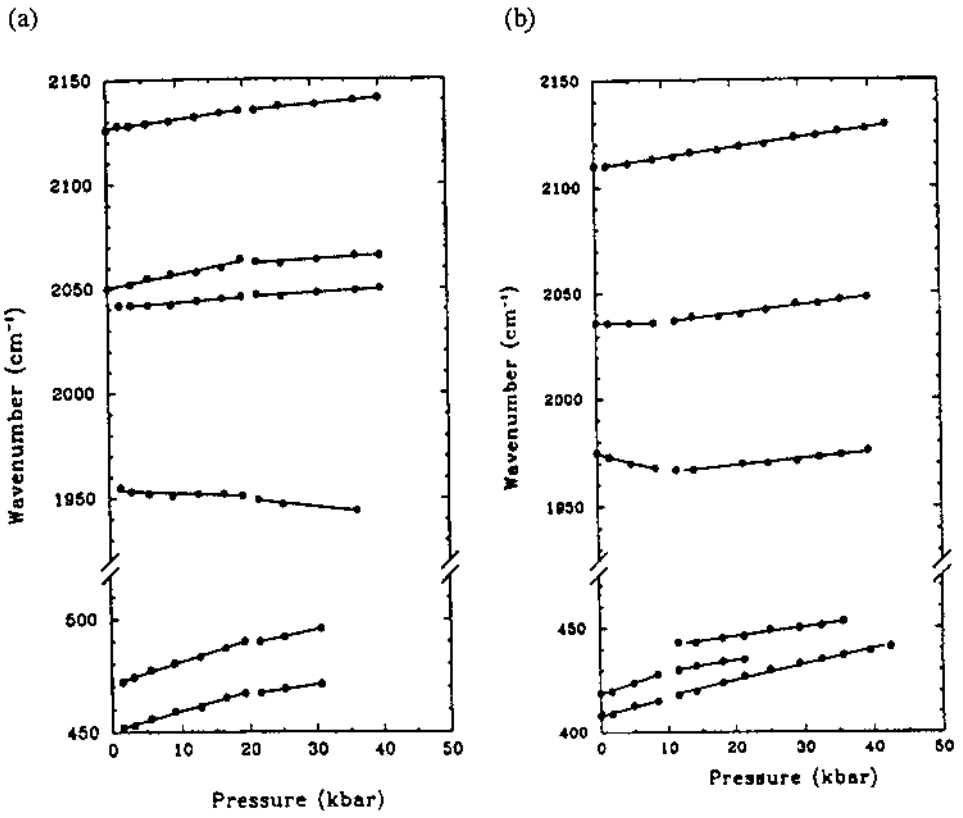

Fig. 5. Pressure dependences of selected Raman bands of (a) $CH_3Mn(CO)_5$ and (b) $CH_3Re(CO)_5$. Reprinted with permission from Y. Huang, I.S. Butler, D.F.R. Gilson, D. Lafleur, Inorg. Chem. 30 (1991) 117. ©1991 American Chemical Society.

$CH_3Re(CO)_5$, on the other hand, showed a negative pressure response over the whole pressure range investigated, becoming more negative after the phase transition: $dv/dp = -0.15$ and -0.33 cm^{-1} kbar^{-1}. These effects are due to the *trans* effect of the methyl group, which is the combination of two opposing tendencies, the π- and σ-effect. McQuillan et al. [30] have calculated a energy-factored force field for the CO stretching vibrations by using gas phase data, including the b_1 fundamental. An a_1 force field for all the vibrations showed that all the M–C bonds increased in strength from Mn to Re while the methyl CH bond was weakened. The axial and equatorial M–CO bonds in $(CH_3)Re(CO)_5$ were found to be equal in strength. McQuillan et al. thus concluded that the π-effect in $(CH_3)Mn(CO)_5$ is greater than is the σ-effect, whereas in $(CH_3)Re(CO)_5$ the two effects are approximately equal and offers a plausible explanation for the observed differences under compression. The π effect strengthens the $M–CO^{ax}$ bond by increasing the population of the axial CO π* orbital through the interaction with the metal d_{xz} and d_{yz} orbitals. The σ-effect weakens the $M–CO^{ax}$ bond because the presence of the

inductive CH_3 group leads to an increase in the electron density at the metal atom through the σ-bond. All the $\nu(M–CO^{ax})$ modes exhibited high positive pressure dependences. These results have been summarized in Table 2. Large positive pressure shifts of the $\nu(CH)$ modes of the CH_3 groups in the IR spectra and a discontinuity at ~ 9 kbar for the manganese complex provided additional evidence for a pressure-induced phase transition in $CH_3Mn(CO)_5$ at this pressure.

High-pressure studies on $M_2(CO)_{10}$ (M = Re, Mn) [31] and $MnRe(CO)_{10}$ [32] present further evidence that the effect of pressure on the axial carbonyl groups is dependent on the nature of the *trans* group. In $Re_2(CO)_{10}$, at the phase transition, which involves a change in geometry from staggered to eclipsed, the Raman-active axial $\nu(CO)$ mode drops by 8 cm^{-1}. Concurrently, the $\nu(Re–C^{ax})$ mode shifts upward by 17 cm^{-1}. These changes imply that, on becoming eclipsed, the π-back-bonding from the rhenium to the axial carbonyl is sharply enhanced. The phase transition in $Mn_2(CO)_{10}$ causes no discontinuity in $\nu(Mn–Mn)$ mode. Dramatic changes in all regions of the Raman spectra were observed at 5 and 8 kbar for $Mn_2(CO)_{10}$ and $Re_2(CO)_{10}$, respectively, consistent with a change in molecular geometry from staggered to eclipsed. $MnRe(CO)_{10}$ differs from its homonuclear analogues in showing two first-order phase changes, at ~ 7 and ~ 13 kbar, involving a change from the staggered to eclipsed and back to staggered geometry. Although the pressure sensitivity of the $\nu(CO)$ modes were smaller by an order of magnitude in the second high-pressure (eclipsed) phase, $d\nu/dp$ was always positive. The electronic spectra of $M_2(CO)_{10}$ (M = Re, Mn) have also been measured under pressure and will be discussed later.

A series of metal tricarbonyl complexes was also investigated to determine the effect, if any, of changing the nature of the ancillary ligand on the metal and the pressure response of the carbonyl ligands. Tricarbonyl(η^5-cyclopentadienyl)rhenium(I), $CpRe(CO)_3$ [33] and the analogous η^5-pentamethylcyclopentadienyl complex, $Cp^*Re(CO)_3$ [34], were studied under applied pressures of 40–60 kbar. Both complexes show a phase transition at ~ 9 kbar, although they are probably of a different nature since they crystallize in different space groups and the increase in intermolecular splitting is greater for the η^5-cyclopentadienyl complex than for the η^5-pentamethylcyclopentadienyl one, as seen from the increased factor group splitting in the former. For $CpRe(CO)_3$, two of the Raman-active *e* $\nu(CO)$ stretching modes, at 1910 and 1904 cm^{-1}, showed negative pressure responses in the low-pressure phase of -0.16 and -0.45 cm^{-1} $kbar^{-1}$, respectively. The third component of the e_1 $\nu(CO)$ mode, at 1935 cm^{-1}, was insensitive to pressure initially, but showed a high, positive pressure dependence, 0.39 cm^{-1} $kbar^{-1}$, in the high-pressure phase. The pressure insensitivity and negative pressure dependence point to an increase in π-backbonding from the rhenium metal to CO, in the low-pressure phase. The other $\nu(CO)$ bands displayed positive pressure dependences. The effect of pressure on the $\nu(CO)$ modes of $Cp^*Re(CO)_3$ was very similar. Only two components of the e_1 $\nu(CO)$ mode were clearly visible, the low frequency band showing a negative shift, $d\nu/dp = -0.22$ cm^{-1} $kbar^{-1}$ in the low-pressure phase but 0.07 cm^{-1} $kbar^{-1}$ in the high-pressure phase. The smaller pressure shifts for the $\nu(CO)$ modes for $Cp^*Re(CO)_3$ compared to $CpRe(CO)_3$ are

Table 2
Pressure dependences of the Raman-active ν(CO) and ν(M–CH_3) modes for $CH_3M(CO)_5$, (M = Re, Mn)

$CH_3Mn(CO)_5$[b]				$CH_3Re(CO)_5$[b]				Assignment
Low-pressure phase		High-pressure phase		Low-pressure phase		High-pressure phase		
ν (cm^{-1})	$d\nu/dp$ ($cm^{-1}kbar^{-1}$)	ν (cm^{-1})	$d\nu/dp$ ($cm^{-1}kbar^{-1}$)	ν (cm^{-1})	$d\nu/dp$ ($cm^{-1}kbar^{-1}$)	ν (cm^{-1})	$d\nu/dp$ ($cm^{-1}kbar^{-1}$)	
2110	0.46	[a]	–	2126	0.44	2135	0.31	ν_2, a_1, $\nu(CO^{eq})$
–	–	–	–	2050	0.69	2063	0.22	ν_{12}, b_1, $\nu(CO^{eq})$
2036	0.00	2037	0.40	2042	0.24	2047	0.19	″
1975	−0.82	1967	0.30	1955	−0.15	1949	−0.33	ν_3, a_1, $\nu(CO^{ax})$
419	1.09	430	0.51	452	0.85	467	0.44	ν_7, a_1, $\nu(MCH_3)$

[a] Indicates no break in the slope at the phase transition.
[b] Ref. [27].

interesting, because, a priori, it would be expected that the pentamethylcyclopentadienyl ligand would be capable of transferring greater electronic charge to the metal center than does the cyclopentadienyl ligand, thereby affording increased π-backbonding to the carbonyl ligands under pressure. These results imply a limitation to the extent of π-backbonding allowed between a metal and a carbonyl ligand. One further point of interest for these compounds is the relatively large $d\nu/dp$ values for the C–Re–C bending modes, which are of the order of 1.38 and 1.76 cm^{-1} $kbar^{-1}$ for the δ(CReC) mode of $CpRe(CO)_5$ and $Cp^*Re(CO)_5$, respectively, implying significant changes in the C–Re–C bond angles under compression.

The thiocarbonyl ligand is also a π-acid like carbonyl but, because of different relative energies of the HOMO and LUMO orbitals of the thiocarbonyl ligand compared to the carbonyl ligand, CS is both a better σ-donor and π-acceptor ligand [35]. But like CO, the metal–CS interactions can be perturbed by the application of pressure and high-pressure studies have been conducted on several thiocarbonyl complexes in order to probe the bonding interactions and study the influence of the ancillary ligands.

For example, $Cr(CO)_5(CS)$, (η^6-C_6H_6)$Cr(CO)_2(CS)$ [36] and $CpMn(CO)_2(CS)$ [37] have been examined under high-pressure by both FT-IR and Raman spectroscopy. The three complexes showed that the effect of pressure was a complicated balance between the effect of compression on the intramolecular distances (which results in a positive shift of all vibrational frequencies) and an increase in the π-backbonding from the metal to the carbonyl or thiocarbonyl ligand. Comparison of the results for $Cr(CO)_5(CS)$ and (η^6-C_6H_6)$Cr(CO)_2(CS)$ indicates that on replacing three carbonyl ligands with an electron donating ancillary ligand, a benzene ring, the extent of π-backbonding increases to all the carbonyl and thiocarbonyl ligands, but that under pressure the increase in π-backbonding to the carbonyls is greater than to the thiocarbonyl ligand (Table 3). Initially, the Cr–CS interactions are stronger than are the Cr–CO interactions, but the results again demonstrate that there is a limit to the amount of electron donation possible through π-backbonding. A recent, high-pressure Raman study on (η^6-$C_6H_5CO_2CH_3$)$Cr(CO)_2(CS)$ [38] has looked at the influence of replacing the benzene ligand with, $-C_6H_5CO_2CH_3$, which has an electron-withdrawing character. The results show that the nature of the ancillary ligand has a large influence on both the extent of π-backbonding to the carbonyl and thiocarbonyl ligands at ambient pressure and the increase in π-backbonding under applied pressure. Substitution of a carbonyl ligand for thiocarbonyl ligand also affects the relative frequencies of the metal-ring vibrations. In (η^6-$C_6H_5CO_2CH_3$)$Cr(CO)_3$, the $\nu(Cr-R)_{sym}$ and $\nu(Cr-R)_{asym}$ modes are at 324.8 and 311.2 cm^{-1}, respectively. For (η^6-$C_6H_5CO_2CH_3$)$Cr(CO)_2(CS)$, these modes are at 318.9 and 280.9 cm^{-1}, respectively. These assignments were made on the basis of relative intensities and pressure dependences of the bands. Compared to the ν(CO) stretch, the ν(CS) stretch revealed a surprisingly high pressure sensitivity. For the complex (η^6-$C_6H_5CO_2CH_3$)$Cr(CO)_2(CS)$, the $d\nu/dp$ values for ν_s(CO) and ν(CS), above $\sim$10 kbar, were 0.17 and 0.63 cm^{-1} $kbar^{-1}$, respectively. Mixing of the ν(CS) mode with the low-energy ν(Cr–CS) mode occurs as a result of their same symmetry, and the large positive pressure dependence for this latter mode contributes positively to the overall pressure sensitivity of the ν(CS) mode.

Table 3
Pressure dependence of selected Raman-active modes

$Cr(CO)_5(CS)$[a]		$(\eta^6$–$C_6H_6)Cr(CO)_2(CS)$[a]		$(\eta^6$-$C_6H_5CO_2CH_3)Cr(CO)_3$[b]		$(\eta^6$-$C_6H_5CO_2CH_3)Cr(CO)_2(CS)$[b]		Assignment
ν (cm^{-1})	$d\nu/dp$ (cm^{-1} $kbar^{-1}$)	ν (cm^{-1})	$d\nu/dp$ (cm^{-1} $kbar^{-1}$)	ν (cm^{-1})	$d\nu/dp$ (cm^{-1} $kbar^{-1}$)[c]	ν (cm^{-1})	$d\nu/dp$ (cm^{-1} $kbar^{-1}$)[c]	
2088[eq]	0.18	1962	0.37	1970	0.03, 0.27	1962	0.01, 0.17	ν(CO)
2017[eq]	0.22	1943	−0.59	1898	0.05, 0.19	1912	−0.03, −0.34	ν(CO)
2017[ax]	−0.18	1908	0.59	1870	−0.03, −0.07			ν(CO)
1989[eq]	−0.53	1856	−0.54	1855	0.08, –			ν(CO)
1289	−0.25	1211	0.85			1205	0.02, 0.63	ν(CS)
1260	−0.09	1192	0.37			1197	1.12	ν(CS)
427[eq]	0.73	452	0.80	480	0, 0.69	452.1	0.017, 0.61	ν(CrCO)
422[ax]	0.82			474	−,0.34			ν(CrCO)
381[eq]	0.78							ν(CrCO)
352	0.70	432	0.41			429	0.04, 0.3	ν(CrCS)
636	−0.46,0.33	646	0.17	663	0.04, 0.46			δ(CrCO)
512	0.16	611	0.33	632	0.05, –	640	0.04, 0.32	δ(CrCO)
487	0.21	600	0.12	623	–			δ(CrCO)
340	–	521	0.21			592	−0.55, –	δ(CrCS)
		502	0.28			524	−0.16, 0.26	δ(CrCS)

[a] Ref. [36].
[b] Ref. [38].
[c] A phase transition was observed in the 10–15 kbar range. The pressure dependence is given for the low-pressure phase and the high-pressure phase.

Another π-acid ligand is *tert*-butyl isocyanide (CNBu-*t*). NMR studies indicate that CNBu-*t* is a better σ-donor, but poorer π-acceptor ligand compared to the carbonyl ligand [39]. Pressure-tuning infrared and Raman spectroscopy have been used to examine the relative π-backbonding capabilities of the CO and CNBu-*t* ligands in chromium(0) complexes [40]. Two complexes were studied, $Cr(CO)_5(CNBu\text{-}t)$ and *cis*-$Cr(CO)_4(CNBu\text{-}t)_2$, both complexes showing a second-order phase transition at ~ 11 and ~ 6 kbar, respectively (Fig. 6). For $Cr(CO)_5(CNBu\text{-}t)$, the equatorial $\nu(CO)$ mode was more pressure sensitive than was the axial $\nu(CO)$ mode, which was essentially independent of pressure below the transition pressure. After the phase change, all three modes (a_1^{ax}, a_1^{eq} and b_1) showed a positive pressure shift of about the same magnitude. The $\nu(CN)$ mode was more pressure sensitive in both the low-pressure and high-pressure phases as a result of the greater anharmonicity of the CN vibration and the larger bulk of the ligand itself. The fact that $d\nu/dp$ $[\nu(CN)] \gg d\nu/dp$ $[\nu(CO)]$ in the low-pressure phase provides further evidence that CNBu-*t* has a lower π-acceptor capability. The results for *cis*-$Cr(CO)_4(CNBu\text{-}t)_2$ further demonstrate the geometrical dependence of the pressure sensitivities of the $\nu(CO^{eq})$ and $\nu(CO^{ax})$ modes. The CO groups *trans* to the CNBu-*t* ligands would be expected to exhibit greater π-backbonding effects

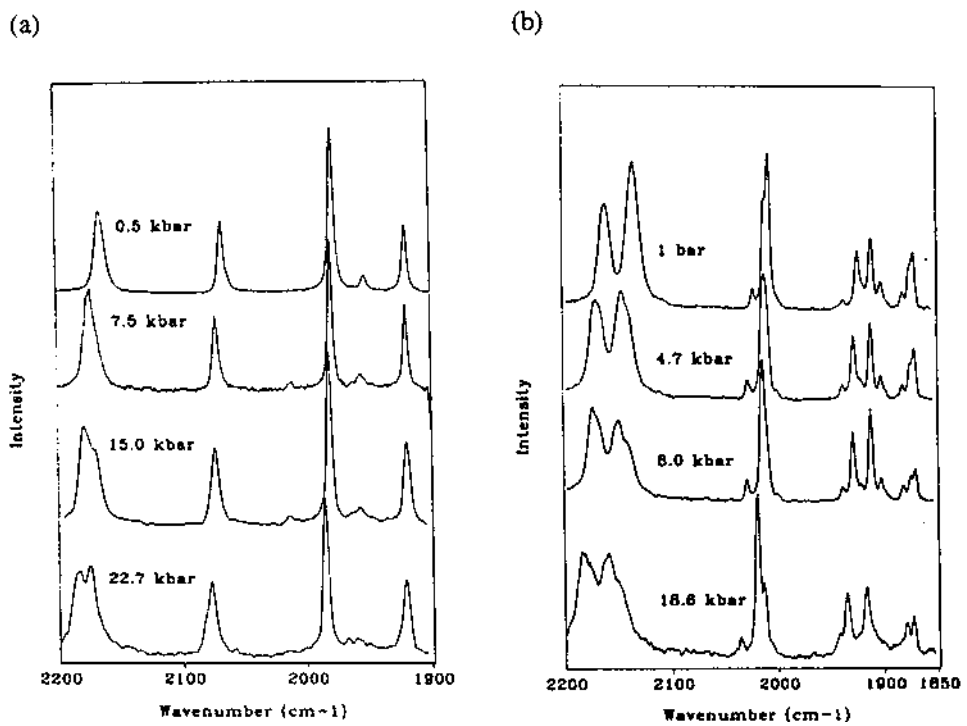

Fig. 6. Raman spectra of (a) $Cr(CO)_5(CNBu\text{-}t)$ and (b) *cis*-$Cr(CO)_4(CNBu\text{-}t)_2$ at four different pressures. Reprinted with permission from H. Li, I.S. Butler, Inorg. Chem. 34 (1995) 1193. ©1995 American Chemical Society.

and therefore have a smaller dv/dp value than do the $v(CO^{eq})$ modes. This is exactly what was observed.

The phase behaviour of several metal–cyano complexes has been studied, and the results show that the metal π–CN π* interactions are increased under compression in a similar manner to those for metal–carbonyl interactions [41]. For instance, $K[Au(CN)_2]$ is one of the most stable and best characterized two-coordinate complexes, with discrete, almost linear [N≡C–Au–C≡N] ions. Phase transitions, indicated by large discontinuities in the pressure sensitivities of the Raman modes, were observed at 6.6 and 10.5 kbar. In phase II, between 6.6 and 10.5 kbar, the v(CN) modes in the 2175–2165 cm^{-1} region showed very strong, negative pressure shifts of -3.43, -3.85 and -3.7 cm^{-1} $kbar^{-1}$. Before and after the phase transition, these modes exhibited typical, positive pressure sensitivities. The first-order phase transition at 6.6 kbar leads to a phase in which the π-backbonding to the CN ligand has a controlling influence on the phase behaviour of the complex.

Metal–alkene bonding interactions also have dual character, the two bonding interactions being synergically related, as for carbonyl ligands. One particularly well-known example of metal–alkene coordination is in Zeise's salt, $K[Pt(\eta^2\text{-}C_2H_4)Cl_3]$. In order for π-backdonation of electrons from the platinum to the π*-orbital on the ethylene to occur, a perpendicular geometry of the ethylene to the $PtCl_3$ plane is required. High-pressure infrared and micro-Raman spectra were recorded for $K[Pt(\eta^2\text{-}C_2H_2)Cl_3]$, the dimer, $[Pt(\eta^2\text{-}C_2H_2)Cl_2]_2$, and dichloro(1,5-cyclooctadiene)platinum(II), $Pt(COD)Cl_2$. Under compression, the extent of π-backbonding increased, as shown by the negative pressure dependences of the peaks attributed primarily to the v(C=C) stretching frequencies [42]. No evidence for a change in the geometry of the alkene was observed.

5.2. Pressure-induced isomerization and piezochromism

When external pressure is applied, the unit cell volume of the system decreases and the intermolecular separations are reduced. The consequence of this is changes in the lattice packing forces, including cation–anion interactions, van der Waals forces and hydrogen-bonding, which determine the specific configuration of the molecule or ion. Under pressure, the delicate balance of the competing molecular forces is disrupted and, if a second configuration of comparable stability exists, solid-state isomerization can be induced.

Coffer et al. have shown that the green form of $[Au_9(PPh_3)_8][PF_6]_3$, which can be viewed as a D_{2h} fragment of an icosahedron **1**,

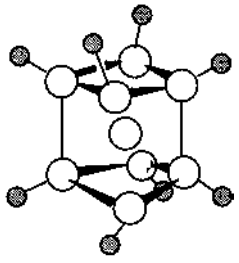

1

can be transformed to the brown form, which has a D_{4d} centered-crown structure **2**

1

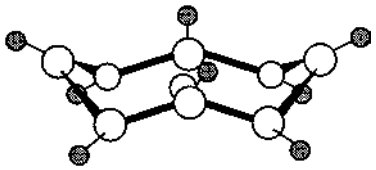

2

[43]. Each form possesses its own distinct electronic absorption spectrum in the solid state and changes in the spectrum of $[Au_9(PPh_3)_8][PF_6]_3$ showed that, over the pressure range 45–60 kbar, isomerization to the brown form occurred. This piezochromic process was reversible and was favored by changing cation–cation and cation–anion intermolecular forces.

$Rh_2(\mu\text{-}Cl)_2(CNC_8H_9)_4(\mu\text{-}AuPPh_3)]_2(PF_6)_2$ **3**

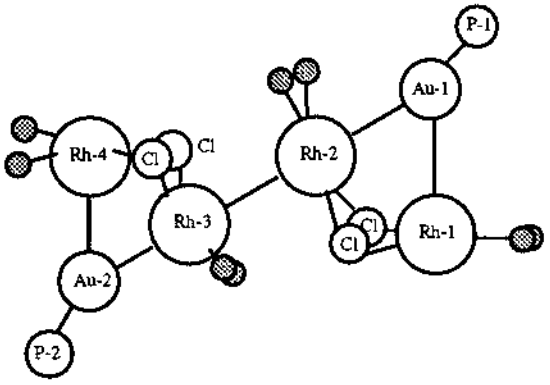

3-*trans*

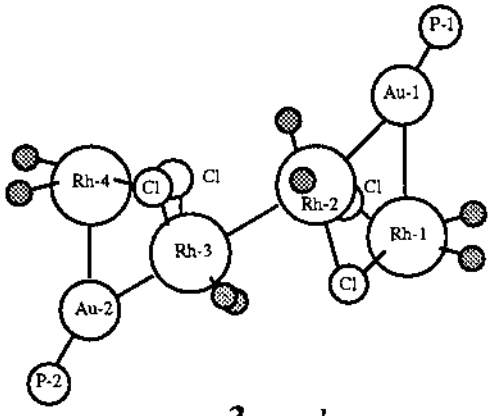

3-*gauche*

= CNC_8H_9

exists as two isomers, a red isomer, in which the two cluster fragments adopt a *trans*, eclipsed conformation about a central Rh–Rh bond, and a green isomer, which has a *gauche*, staggered conformation. Pressure-dependent electronic spectroscopy indicates that the two isomers become geometrically similar at high pressures, by inducing a conformational change around the Rh–Rh bond [44].

Piezochromism has been observed in a large number of Cu(II) complexes, containing a large variety of ligands [45]. For example, complexes of the type $[CuL_2]X_2$ [L = *N*,*N*-diethylethylenediamine (dieten), ethylenediamine (en), X = BF_4^-] adopt an elongated, tetragonal octahedral configuration with an approximately planar CuN_4 arrangement and the anions occupying symmetric sites above and below the CuN_4 plane **4**.

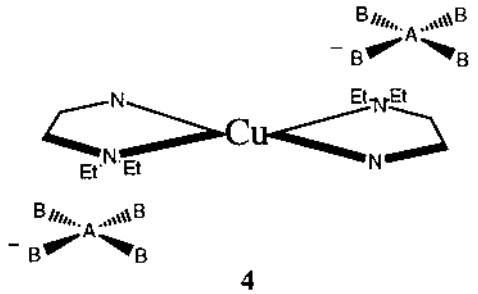

4

When L is en, the anions lie perpendicular to the plane passing through the copper cation. When L is dieten, the anions lie off this perpendicular. Under pressure [46], a molecular rearrangement in $[Cu(dieten)_2](BF_4)_2$ occurs in which a marked decrease in the anion-molecular plane distance results, with a concomitant increase in the interaction between the anion and cation. These changes appear as significant shifts in the bands of the electronic spectrum as the d_{z^2} orbital of copper interacts with the anion, and changes in the IR spectra, which correspond to a lowering of the symmetry of the tetrahedral anion (Fig. 7). At higher pressures, the structure of the dieten complex becomes more like the ambient pressure structure of the en complexes.

Copper complexes of the type $[Cu(dien)(bipyam)]X_2 \cdot nH_2O$ (dien = diethylenetriamine, bipyam = 2,2′-dipyridylamine; X = Cl^-, ClO_4^-, NO_3^-) show continuous transformations from distorted trigonal-bypyramidal structures to regular square-pyramidal conformations under the application of pressure [47]. Again, the electronic and IR spectra provided evidence for pressure-induced configuration rearrangements in these complexes. The one-electron energy levels of the Cu(II) ions in various geometries, and with various ligands, are well documented and highly characteristic of the geometry about the Cu(II) center. Other five-coordinate Cu^{2+} complexes show the same behavior under compression [48].

In the tetrachlorocuprate anion, $[CuCl_4]^{2-}$, the dihedral angle can vary such that geometries from nearly tetrahedral to square planar are possible, simply on changing the cation. Bray and Drickamer have studied the effect of compression on the electronic spectra of a range of $X^{2+}[CuCl_4]^{2-}$ complexes [49]. They found that complexes with a large dihedral angle at ambient pressure, e.g. $Cs_2[CuCl_4]$, tended

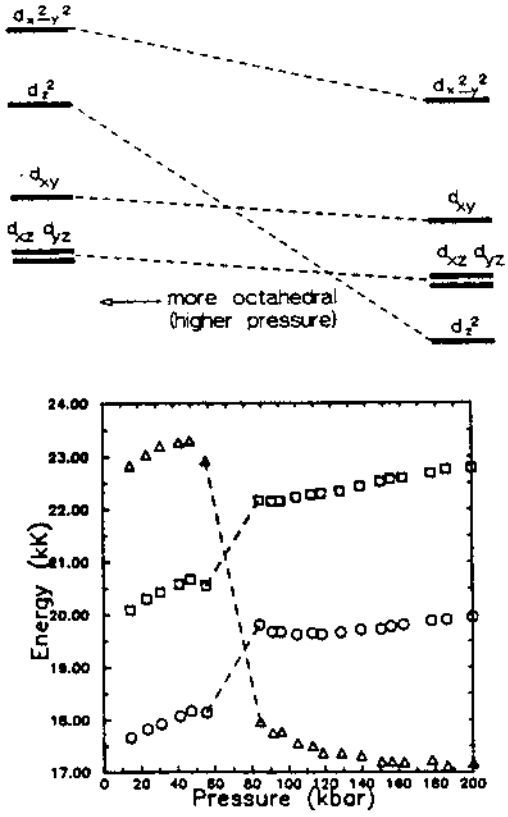

Fig. 7. Splitting of the one-electron orbitals of the d^9, Cu^{2+} cation in D_{4h} symmetry and the pressure dependences of the energies of the $d_{z^2} \rightarrow d_{x^2-y^2}$ (△), d_{xz}, $d_{yz} \rightarrow d_{x^2-y^2}$ (○), and $d_{xy} \rightarrow d_{x^2-y^2}$ (□) electronic transitions in polycrystalline $[Cu(dieten)_2](BF_4)_2$. Reprinted with permission from K.L. Bray, H.G. Drickamer, E.A. Schmitt, D.N. Hendrickson, J. Am. Chem. Soc. 111 (1989) 2849. ©1989 American Chemical Society.

to show a decrease in dihedral angle under pressure, but a complex with a smaller dihedral angle, e.g. $[(nmpH)_2][CuCl_4]$ (nmpH = *N*-methylphenethylammonuim), showed an increase in dihedral angle. The general result was that, at higher pressures, there was a much smaller range of dihedral angles for the complexes, with neither the tetrahedral or square-planar geometry being the pressure-stabilized configuration of the $[CuCl_4]^{2-}$ ion.

The interconversion of a metal–dihydride $[M-(H)_2]$ to a metal–dihydrogen complex $[M-(\eta^2\text{-}H_2)]$ occurs in several complexes in solution and has been demonstrated by ^{1}H-NMR spectroscopy [50]. It has recently been shown that the dihydride to dihydrogen isomerization can be induced under compression at room temperature, in the solid state [51]. $[(PP_3)Co(H)_2]X$ $[PP_3 = P(C_2H_4PPh_2)_3]$ contains two hydride ligands when co-crystallized with the BPh_4^- counterion, but shows the dihydrogen form when PF_6^- is the counterion (Scheme 1). In solution the dihydride

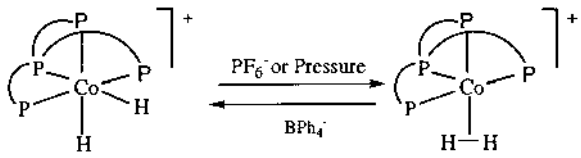

Scheme 1.

is the stable form, regardless of anion. The dihydride complex is pale yellow while the dihydrogen complex is red. Under modest pressures of just 6–10 kbar, the pale yellow dihydride complex $[(PP_3)Co(H)_2]BPh_4$ is transformed into the red dihydrogen complex. The isomerization was seen visually by observing the color change, in the visible spectrum (Fig. 8), and in the FT-IR spectrum. A disappearance of the ν(CoH) stretching mode, at 1866 cm^{-1} at ambient pressure, was observed at the transition pressure. A neutral rhenium heptahydride complex, ReH_7(dppe) [dppe = 1,2-bis(diphenylphosphino)ethane], showed a similar transition under compression

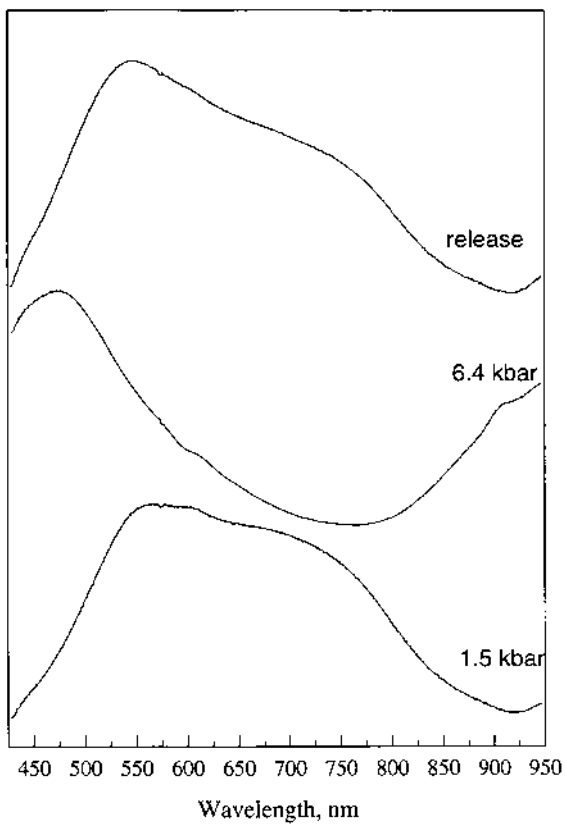

Fig. 8. Compression and decompression visible absorption spectra of $[(PP_3)Co(H)_2]BPh_4$ (PP_3 = $P(C_2H_4PPh_2)_3$).

[52]. At ~10 kbar, a broad band centered at 2640 cm^{-1} was observed in the spectrum, this band gaining some intensity with further increases in pressure. From the neutron diffraction structure at ambient pressure, two of the hydride ligands lie closer to one another than do the others and it is likely that under compression these two hydrides come into closer proximity to form a dihydrogen bond. The frequency of the ν(HH) mode of the η^2-H_2 ligand suggests a short H–H distance of the order 0.8–0.95 Å, when compared to frequencies reported in the literature [53]. For many Re–(η^2-H_2) complexes, d(H–H) is generally observed to be considerably longer, at ~1.3 Å [54]. $Cp^*Ir(PMe_3)(H)_2$ showed no changes in the FT-IR spectra, under compression, to suggest dihydrogen formation [55]. All the IR modes hardened under pressure and no break was observed in the wavenumber versus pressure plots. The above results are of particular interest as there is considerable discussion on the importance of steric versus electronic effects and the stability of the dihydrogen ligand.

5.3. Metal–metal bonds under compression

The metal–metal quadruple bond is typified by $[ReCl_8]^{2-}$, which has an eclipsed conformation of the two ML_4 halves, despite the resulting steric effects. High-pressure applied to salts of both $[ReBr_8]^{2-}$ and $[ReI_8]^{2-}$ causes torsion from an eclipsed to a staggered conformation [56–58]. With increasing pressure, a new band appears in the visible spectrum, red-shifted from the well-known $\delta \rightarrow \delta^*$ transition of the eclipsed form. The new, low-energy peak is assigned to $\delta \rightarrow \delta^*$ transition of the staggered conformation. The transformation from eclipsed to staggered results in zero overlap of the $d_{xy} - d_{xy}$ orbitals. Morris et al. have studied the electronic and resonance Raman spectra of the eclipsed $[Re_2X_8]^{2-}$ (X = F, Cl, Br) species, as well as those of the complex $Mo_2Cl_4(PMe_3)_4$, whose D_{2d} interlocked phosphine-ligand geometry contributes considerable torsional rigidity up to 15 kbar [59]. The $\nu(Re_2)$ mode for $Re_2X_8^{2-}$ in dichloromethane and $\nu(Mo_2)$ for $Mo_2Cl_4(PMe_3)_4$ in cyclohexane showed a continuous increase in frequency with increasing pressure. The shift in $\nu(Re_2)$ is dependent on X, with F > Cl > Br. The shortening of the metal–metal bond was significant in all the complexes. The change in Mo–Mo bond length was intermediate between the bond length change in the $[Re_2Cl_8]^{2-}$ and $[Re_2Br_8]^{2-}$ complexes. Although the PMe_3 ligands are larger than are the halide ligands, the D_{2d}-interlocked phosphine geometry mitigates this effect. The electronic spectra (in solution) showed a continuous shift to lower wavenumbers. No new bands were observed, as reported by Carroll et al. [56]. The bands did broaden and changes in intensity were noted. A pressure-induced torsional distortion was thought to occur in all three rhenium complexes, although $[Re_2Cl_8]^{2-}$ and $[Re_2Br_8]^{2-}$ had a greater tendency to distort. The molybdenum complex, on the other hand, did not undergo torsional distortion, presumably due to steric repulsion of the tertiary phosphine ligands.

As mentioned earlier, the decacarbonyl complexes, $Mn_2(CO)_{10}$ and $Re_2(CO)_{10}$ have a staggered conformation in the solid state, at ambient pressure, with a direct, unbridged metal–metal bond. Upon the application of pressure, the IR spectra

show changes consistent with a change in symmetry from D_{4d} to D_{4h} (Fig. 9) [31]. The transition observed at ~ 5 kbar for $Re_2(CO)_{10}$ and ~ 8 kbar for $Mn_2(CO)_{10}$ is due to torsion about the M–M bond to the eclipsed conformation. Pressure-tuning of the electronic states of $Mn_2(CO)_{10}$ and $Re_2(CO)_{10}$ has also been investigated [60] but, since the electronic states have cylindrical symmetry, the phase transition from the staggered to eclipsed form was not detected. For both molecules the highest filled orbital is a σ (bonding) orbital while the lowest unoccupied orbital is a σ^* (antibonding) orbital. The $\sigma \rightarrow \sigma^*$ transition in the crystalline state initially blue shifts at about 50 and 17 cm^{-1} $kbar^{-1}$ for $Mn_2(CO)_{10}$ and $Re_2(CO)_{10}$, respectively, showing that the dominant pressure effect is stabilization of the bonding orbital relative to the antibonding are because of increased orbital overlap. In solution, the initial shift of the $\sigma \rightarrow \sigma^*$ transition was reduced for $Re_2(CO)_{10}$ when ethanol was replaced by the more polarizable solvent dichloromethane. In ethanol, the shifts in the $\sigma \rightarrow \sigma^*$ transition for $Mn_2(CO)_{10}$ and $Re_2(CO)_{10}$ were similar in magnitude and direction. This latter result shows that since the effect of pressure was the same in

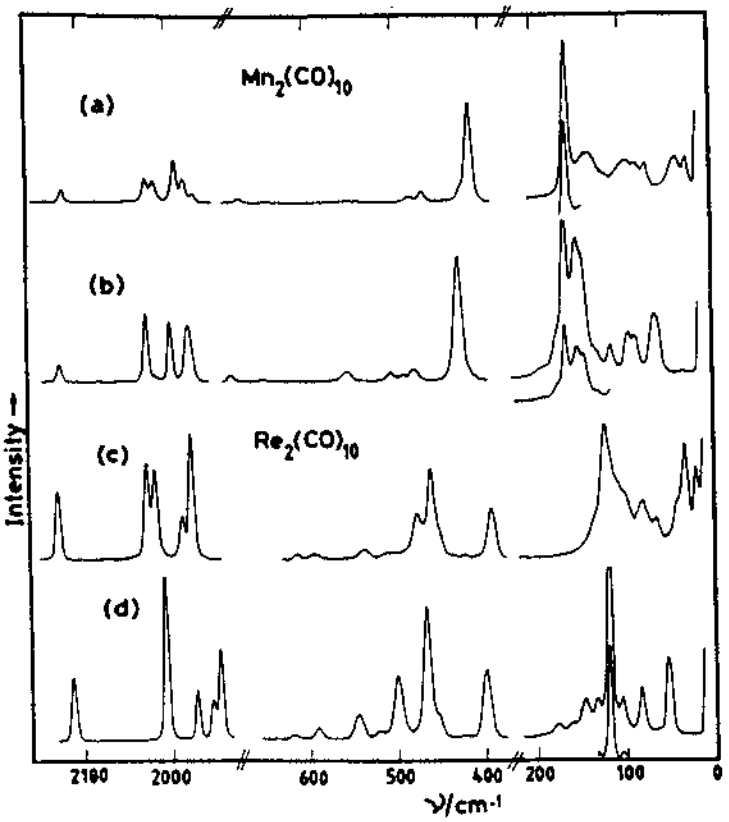

Fig. 9. Raman spectrum of $Mn_2(CO)_{10}$ at (a) ambient pressure, (b) 16 kbar, and of $Re_2(CO)_{10}$ at (c) ambient pressure and (d) 16 kbar. Reprinted with permission from D.M. Adams, P.D. Hatton, A.C. Shaw, J. Phys., Condens. Matter 3 (1991) 6145.

ethanol for each compound the differences in the solid state must be due to intermolecular interactions.

Breaks in the wavenumber versus pressure plots for the IR modes of $Mn_2(CO)_{10}$ indicate two phase transitions at ~ 7 and ~ 13 kbar. The low and high-pressure phases have very similar spectra, while the middle phase, between 7–13 kbar, has a significantly different IR spectrum [32]. The ν(Mn–Re) mode was particularly sensitive to the phase transition, disappearing at 7 kbar, and a new band appearing at ~ 10 cm^{-1} lower. At 13 kbar, this band showed a discontinuous shift of $+8$ cm^{-1}. These changes suggest a transition from the staggered conformation to the eclipsed form at 7 kbar and then back to the staggered conformation at pressures above 13 kbar, with a shortening of the Mn–Re bond distance in the eclipsed conformation. The $M(CO)_5$ units have C_{4v} symmetry in both the staggered and eclipsed conformations and so the symmetry of the ν(CO) modes are insensitive to the transition.

Dihalotetrakis(pivalalto)dirhenium(III) contains a Re–Re quadruple bond. The electronic absorption spectra and high-pressure IR spectra in the 1800–700 cm^{-1} region of $Re_2(piv)_4Cl_2$ and $Re_2(piv)_4Br_2$ ($piv = O_2CCMe_3$) for both the crystalline solids and the complexes dispersed in a polymer matrix were recorded [61]. In the electronic spectra, a new band was observed to grow from ambient pressure on the low-energy side of the $\delta \rightarrow \delta^*$ excitation (Fig. 10). Only above 40 kbar was a decrease in the $\delta \rightarrow \delta^*$ excitation band noted. In the IR spectra, three new bands were observed at 1134, 1280 and 1697 cm^{-1} for X = Br and 1142, 1286 and 1697 cm^{-1} for X = Cl. Since the results were the same for both the crystalline solids and the complex dispersed in polymer, the pressure-induced changes were attributed to intramolecular changes, most probably a change in the coordination of one of the pivalato ligands from bidentate to monodentate, as shown in Scheme 2. The new IR band at 1697 cm^{-1} is assigned to the ν(CO) vibration of the ketone. Other complexes have shown similar behaviour upon chemical changes [62,63]. When $Mo_2(O_2CCF_3)_4$ is reacted with triphenylphosphine the complex $Mo_2(O_2CCF_3)_4(PPh_3)_2$, with PPh_3 occupying the axial position, is formed (Mo–Mo = 2.100(1) Å) [61]. However, when the phosphine ligand is $PPhEt_2$, the phosphine occupies an equatorial site (Mo–Mo = 2.107 Å) and a bridging RCO_2^- as well as monodentate RCO_2^- group is present, these groups being easily identified from an inspection of the CO stretching region (1700–1400 cm^{-1}) in the IR spectrum.

Metal clusters, in particular organometallic carbonyl clusters, have been employed as structural models for adsorbed organic species on metal surfaces. Infrared measurements of molecules adsorbed to metal surfaces have been used to complement data from other surface techniques, such as high-resolution electron energy loss spectroscopy (HREELS). Pressure-tuning spectroscopy on clusters has been useful in the assignment of vibrational bands of adsorbed species. Coffer et al. [64] have studied a series of triosmium clusters with coordinated C_2 hydrocarbon ligands under high-pressures up to 96 kbar. They found that for complex **5**

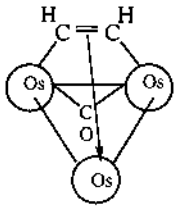

5

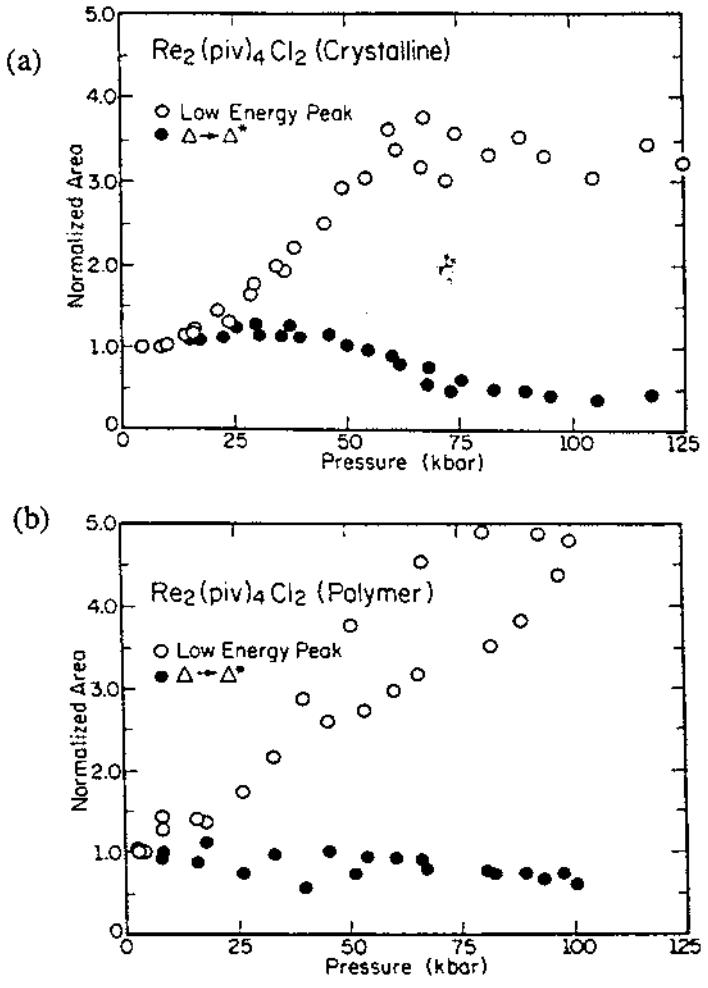

Fig. 10. Area of the low-energy peak (normalized to 1 atm) and of the $\delta \rightarrow \delta^*$ peak in polycrystalline $Re_2(piv)_4Cl_2$ (a) and of $Re_2(piv)_4Cl_2$ in a PMMA matrix (b). Reprinted with permission from R.T. Roginski, T.L. Carroll, A. Moroz, B.R. Whittlesey, J.R. Shapley, H.G. Drickamer, Inorg. Chem. 27 (1988) 3701. ©1988 American Chemical Society.

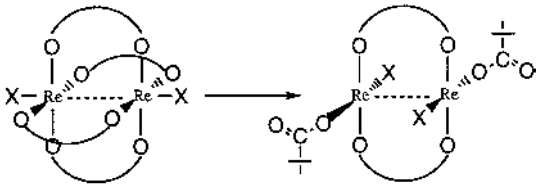

Scheme 2.

the pressure dependences of the bands follow the order C–H stretch > C–C stretch > C–H bend, with all bands typically shifting to higher energy. For clusters **6** and **7**,

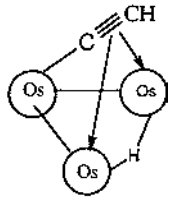

6

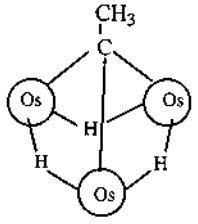

7

the order changed to C–C stretch > C–H stretch > C–H bend, if the shifts were considered in terms of percent change. It was also found that the shift of the C–C stretch was proportional to the frequency of the mode at ambient pressure. A similar high-pressure IR study on the α-pyridyl moiety in $HOs_3(CO)_{10}(\mu,\eta^2\text{-}NC_5H_4)$ to 70 kbar also showed that the $d\nu/dp$ values varied as $\nu(CC) > \delta(CH)$ [65].

Metal–sulfido clusters are of interest, in particular $M_6(\mu_3\text{-}S)_8(PEt_3)_6^{n+}$ (M = Fe, $n = 2$; M = Co, $n = 1, 0$), due to their structural similarity to clusters present in the bulk metal sulfides known as Chevrel phases. The chief structural feature of Chevrel phases is that they contain Mo_6 clusters-the origin of their superconductivity being the Mo 4d electrons, which are strongly localized in the Mo_6 clusters [66]. Pressure-tuning spectroscopy has been used to probe the electronic structure of the metal–sulfido clusters [67]. Compared to the iron cluster, the cobalt cluster showed a much smaller pressure dependence, attributed to weaker M–M interactions and a more delocalized ligand character of the frontier orbitals. The large blue shifts of the observed peaks were attributed to intramolecular effects since the same shifts

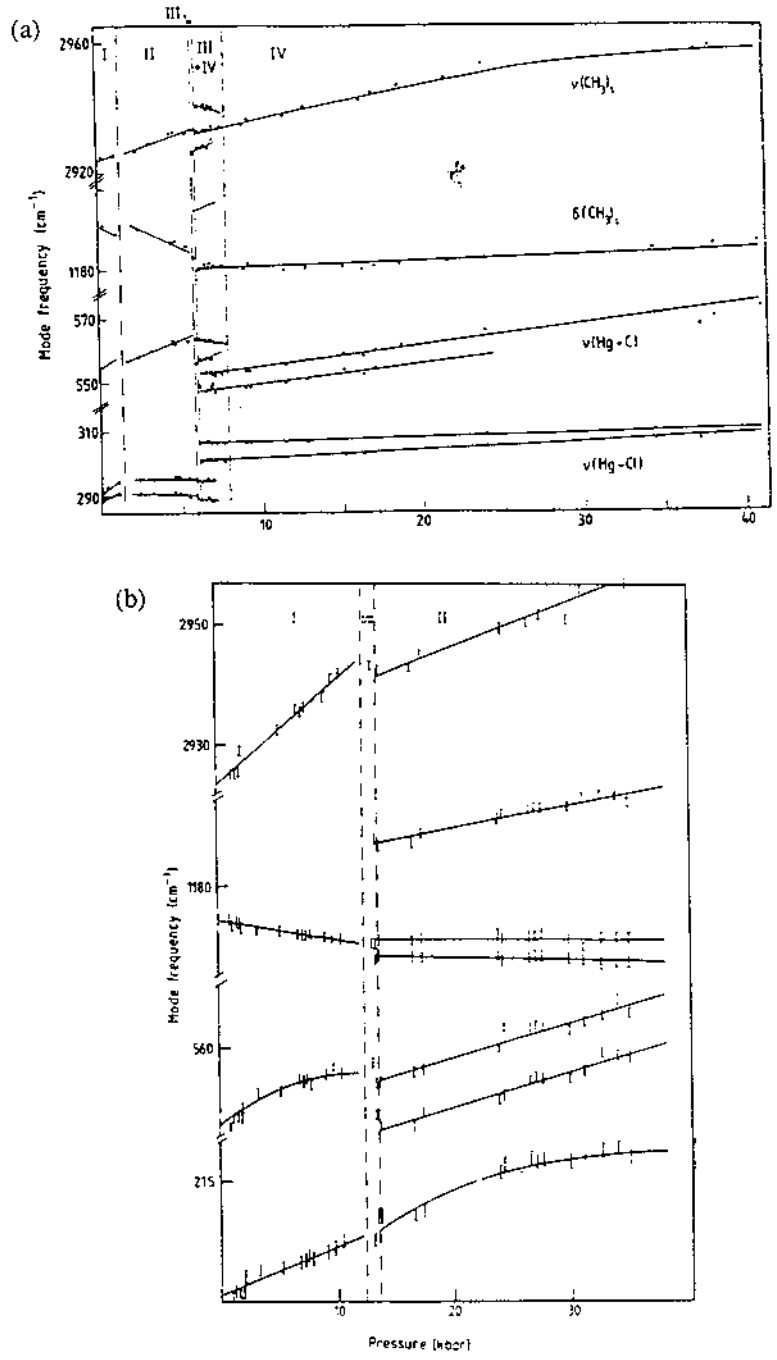

Fig. 11. Wavenumber versus pressure plots for the internal modes of (a) CH_3HgCl; (b) CH_3HgBr; and (c) CH_3HgI. Reprinted with permission from D.M. Adams, M. Pogson, J. Phys. C Solid State Phys. 21 (1988) 1065.

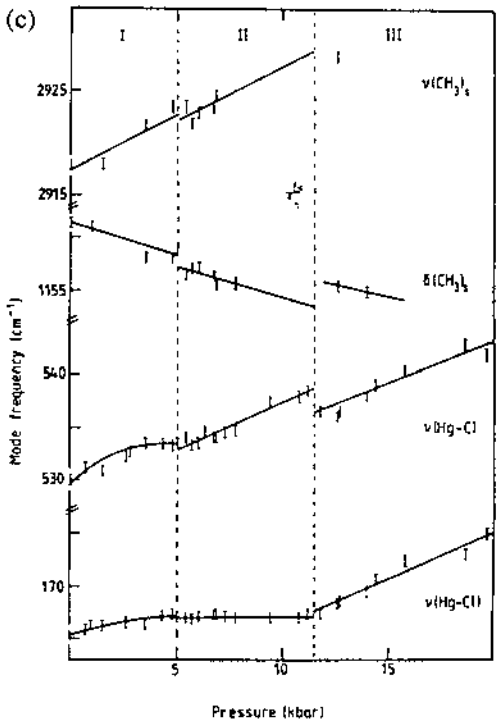

Fig. 11. (*Continued*)

were observed for $Fe_6(\mu_3\text{-}S)_8(PEt_3)_6^{2+}$ dissolved in PMMA and for the crystalline form.

5.4. Order–disorder phenomena under pressure

Solid-state order–disorder transitions in compounds containing CH_3 or NH_3 groups can occur with temperature or pressure and involve molecular internal torsion, much like, for example, the pressure-induced torsion about the M–M bond in $Mn_2(CO)_{10}$ discussed earlier. A Raman study of the phase behavior of CH_3HgX (X = Cl, Br, I) molecules has been carried out up to pressures of 40 kbar [68]. For CH_3HgCl, three phase transitions were observed from the Raman measurements at $\sim$1.5, 5.9 and again at $\sim$6 kbar. Above 8 kbar, there was a single phase present which was stable up to 40 kbar (Fig. 11a). Three Becke lines were observed in an ungasketed pressure experiment, which confirm the transitions as first-order. Becke lines arise form the combination of reflected and refracted light rays at the junction of two materials whose refractive indices are close in magnitude. CH_3HgBr showed a single transition at 12.5 kbar, seen readily in plots of Raman wavenumber versus pressure (Fig. 11b). Two Becke lines were observed for CH_3HgI, with the two phase transitions at 5.0 and 11.5 kbar (Fig. 11c). In all three materials, the increase in

pressure caused significant softening of the $\delta_s(CH_3)$ mode. For the chloride and bromide, in the high-pressure phases, this mode hardened with increasing pressures, while for the iodide the $\delta_s(CH_3)$ mode continued to soften under pressure. The crystal structure determined for CH_3HgCl has a tetragonal space group, which is incompatible with the methyl groups and hence they must be disordered, i.e. there is unrestricted rotation about the Hg–C bond. The crystal structure of CH_3HgBr is similar but there is a definite departure from linearity in the C–Hg–Br skeleton. The methyl groups could be ordered or disordered. CH_3HgI has a crystal structure which is different again. The pronounced softening of the $\delta_s(CH_3)$ mode indicates that the methyl groups are implicated in the phase transition. The I–II phase transition results in cell doubling. In the high pressure phase III + IV of CH_3HgCl, the spectral complexity increases, with new ν(CH), $\delta(CH_3)$ and ν(Hg–Cl) bands appearing. These modes were thought to originate from IR components, indicating a loss of the center of symmetry at the II–III transition. The results also indicate that, during the transition to phase III of CH_3HgCl, the methyl groups cease to be in essentially freely rotating and become fixed.

The methyl groups in dimethyltin difluoride, $(CH_3)_2SnF_2$, lie along the four-fold crystal axis and have been shown to be freely rotating with a low barrier to rotation of less than a few tenths of 1 kcal [69]. A structural phase transition at low-temperature (70.4 K) has been observed by heat capacity, NMR and various neutron scattering techniques and has been confirmed to be second order [70]. The transition is described as instantaneous three-fold jumps of the methyl groups. All the IR and Raman modes harden under compression [71]. At $\sim$40 kbar, the $d\nu/dp$ values change quite significantly for the IR-active symmetric and antisymmetric $\delta(CH_3)$ modes, and becoming essentially zero, indicating that, above the transition pressure, the motion involved with this vibration is less restricted. A shoulder on the degenerate $\delta_{as}(CH_3)$ mode becomes clear above the transition. At higher pressures, restricted rotation of the methyl groups is limited and they become ordered, since the interactions between the methyl groups increase as the molecules are packed closer together.

The $(CH_3)_2TlX$ (X = Cl, Br, I) complexes have been similarly investigated at high-pressures [72]. High-pressure IR and Raman spectra revealed a phase transition in all three complexes. The transition occurred at $\sim$15 kbar for the chloride and just below 10 kbar for the bromide and iodide and involved ordering of the methyl groups. A shoulder on the $\delta_s(CH_3)$ mode became clear above the transition pressure. A second transition was observed at higher pressures, 25 kbar for the chloride, 27 kbar for the iodide, and 45 kbar for the bromide. This second transition involved a doubling of the unit cell and bending of the $(CH_3)_2Tl^+$ ions. The transitions were accompanied by significant changes in the Raman and IR spectra, including dramatic changes in the lattice region for the bromide and iodide. These changes were indicative of a disruption of the $(TlCl)_n$ layers. This was not observed for the chloride.

The NH_3 groups in the hexaamminenickel(II) halides, $[Ni(NH_3)_6]X_2$ (X = Cl, Br, I), have considerable rotational freedom at ambient pressure. Several high-pressure investigations using a variety of methods have detected phase transitions in all three

complexes. Electronic spectroscopy indicated a phase transition at ~ 70 kbar [73], while a phase transition at 27 K and 5.6 kbar was observed in $[Ni(NH_3)_6]I_2$ by inelastic neutron scattering [74]. Far-IR measurements for hexaamminenickel(II) and -cobalt(III) halides under compression also revealed phase transitions, which involved a lowering of symmetry [75]. No explanation for the nature of these transitions was proposed.

A more recent high-pressure IR investigation of the $[Ni(NH_3)_6]X_2$ (X = Cl, Br, I) complexes under hydrostatic conditions was undertaken to obtain a better understanding of their phase-transition behavior [76]. In all three compounds, the $\nu_{as}(NH)$ and $\rho(NH)$ modes shifted to higher wavenumbers with increasing pressure, while the two NH_3 bending modes showed negative pressure dependences (Fig. 12). The magnitude of the pressure shift for the $\delta_s(NH_3)$ mode, -0.75 to -0.9 cm^{-1} $kbar^{-1}$, was much greater than is usually observed for bending modes under compression, indicating that this mode is strongly coupled to a soft mode. A phase transition, detected by the splitting of the vibrational bands, was observed close to 51 kbar for X = Cl and Br and 23 kbar for X = I. New bands were noticed, particularly on the high wavenumber side of the $\delta_s(NH_3)$ mode, which gained intensity with further increases in pressure. Less splitting in the iodide complex indicated a higher symmetry in the high-pressure phase of this complex compared to the chloride and bromide complexes. This splitting of the internal modes of the $-NH_3$ group indicates that the transition involves an ordering of the $-NH_3$ groups. A similar effect was observed at low temperatures, but the low-temperature and high-pressure phases are not the same.

Ferrocene (Cp_2Fe) and other metallocenes exhibit phase transitions with changes in temperature, generally of the order–disorder genre, involving rotational disorder of the π-cyclopentadienyl (Cp) ring and/or reorientational mechanisms. For example, at 169 K there is an order–disorder phase change in ferrocene (Cp_2Fe), followed at 163.9 K by a first-order structural phase change to ferrocene-II [77]. The initial IR spectrum of ferrocene at pressures up to 50 kbar showed a sluggish phase change between 10 and 16.5 kbar [78]. The most dramatic changes were observed for three bands normally inactive under strict D_{5h} symmetry, but which are permitted in the solid state. These bands show a continuous increase in intensity with increasing pressures. The infrared spectrum of $[Cp_2Fe]PF_6$ was recorded at various pressures up to 85 kbar [79]. Three modes in particular showed interesting behavior under pressure (Fig. 13). The CH bend, ν_5, displayed a discontinuous change between 4.8 and 5.5 kbar. The CH bend, ν_3, split into a doublet in the same pressure regime and a band at 1347 cm^{-1} showed a dramatic increase in intensity between 4.8 and 5.5 kbar. The intensity changed very little above 5.5 kbar. Discontinuities in the pressure shift of the electronic transition bands were also observed below 10 kbar [79]. The dramatic changes in the IR spectra suggested that the mechanism for this transition perhaps involved orientational order–disorder for the Cp_2Fe^+ cation. The solid-state IR spectra of ferrocene, Cp_2Fe, nickelocene, Cp_2Ni, and ruthenocene, Cp_2Ru, exhibit significant changes upon compression to 120 kbar [80]. The CH bend, ν_5, shows a large continuous increase in intensity with pressure, except for Cp_2Ru, in which a splitting of the band to a doublet is

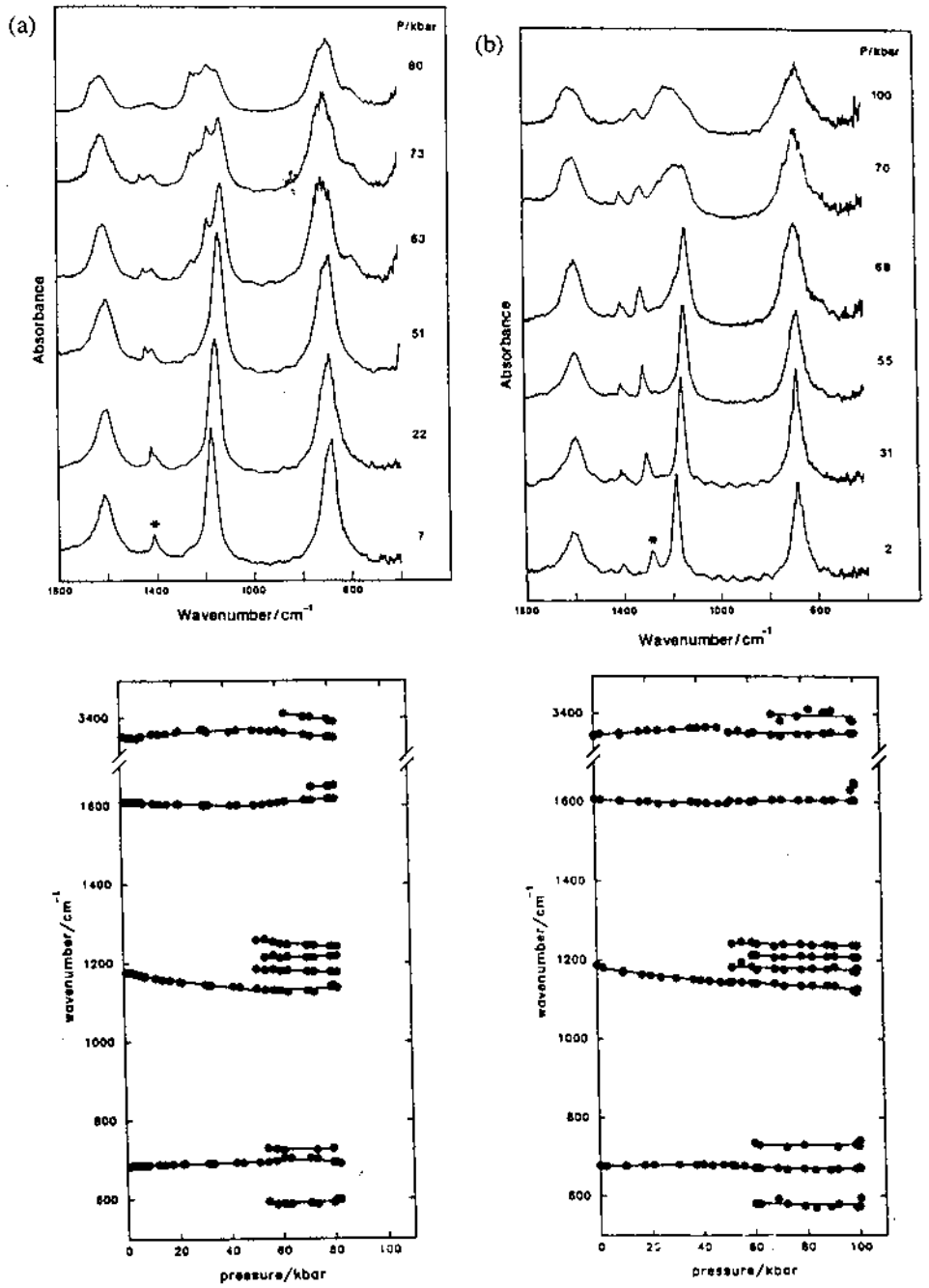

Fig. 12. Infrared spectra at various pressures and the pressure dependence of selected IR modes of (a) $[Ni(NH_3)_6]Cl_2$ and (b) $[Ni(NH_3)_6]Br_2$. *, ν_3 of NO_3^-. Reprinted with permission from D.M. Adams, J. Haines, J. Phys. Chem. 95 (1991) 7068. ©1991 American Chemical Society.

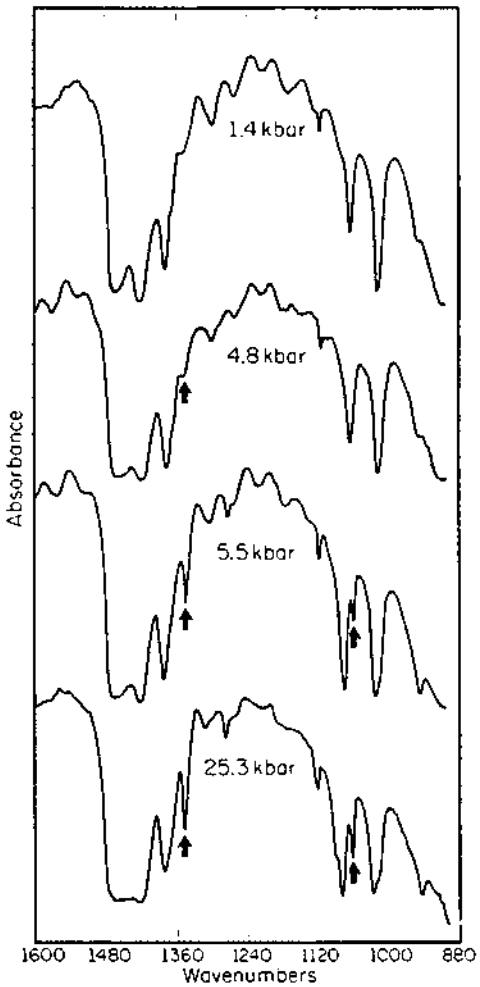

Fig. 13. Portion of the IR spectrum of polycrystalline $[Cp_2Fe]PF_6$ at four different pressures. Reprinted from R.T. Roginski, A. Moroz, H.G. Drickamer, Chem. Phys. Lett. 143 (1988) 577, with kind permission of Elsevier Science-NL, Sara Burgerhartstraat 25, 1055 KV Amsterdam, The Netherlands.

observed. The antisymmetric ring breathing mode broadens considerably, as does the CH bend, ν_{18}, the latter eventually splits into a doublet for Cp_2Fe and a triplet for Cp_2Ni and Cp_2Ru at high pressures. These observations have been explained by considering the result of increased intermolecular coupling, since there are at least two molecules per unit cell and there exist several coincidences between the IR and Raman frequencies. If there is an intermolecular interaction that couples vibrational motions of the two molecules, a vibration, which is normally only Raman active, may become dipole allowed and appear in the IR. As the coupling increases, already dipole-allowed modes will be affected and increase in intensity. This model

was used to explain the observed changes of the increasing intensity of certain bands and a broadening of others. New bands observed in the 900–800 cm^{-1} region at higher pressures are coincident with normally Raman-active modes at ambient pressure. The observed changes for the Cp_2Fe^+ cation must then also involve an increase in intermolecular coupling.

It appears that under compression, ligands that which normally exhibit free rotation under ambient conditions, become ordered most likely as a result of increased intermolecular interactions.

5.5. Pressure-tuning of quasi one-dimensional materials

In halogen-bridged, mixed-valence complexes of the general composition $[ML_4][MX_2L_4]Y_4$, a linear chain forms with alternating long and short metal-to-halogen bonds:$Pt^{II}–Br–Pt^{IV}–Br–Pt^{II}–Br–Pt^{IV}–Br–Pt^{II}–Br–Pt^{IV}–Br–$. A network of ligands and ions forms a template to which the metal and X atoms tend to adjust to along the chain. The choice of L and Y will dramatically influence the separation between metal atoms, which appears to determine Peierls distortion, ρ (the ratio of the short-to-long M–X bond lengths) and the charge-density wave (CDW) state. The Raman-active chain mode, ν_1, associated with the symmetric M–X vibration of Pt^{IV} and the energy of the bandgap, E_g, increase monotonically as ρ decreases. The application of hydrostatic pressure is an ideal method for tuning ρ. A combination of absorption and Raman spectroscopies, and diffraction techniques, along with conductivity measurements, has been used to study the structure and CDW state of these linear chain complexes under applied pressure. These materials are of interest because of their semi-conductor properties; the cyanoplatinate compounds possess nearly metallic electrical conductivities. These complexes have also aided in the development of the theory of the one-dimensional state, 1-D conduction properties, and associated phenomena such as Peierls distortions and CDW.

A series of complexes of the type $M(A)X_3$ [M = Pd, Pt; A = $(NH_3)_2$, $(C_2H_5NH_2)_4$, en, and X = Cl, Br, I] has been studied under compression over a wide range of pressures up to $\sim$150 kbar [81]. Conductivity measurements under pressure showed an increase in conductivity for all the different types of complex. The rate of increase and a leveling off of the conductivity at higher pressures was shown to be dependent on the metal, ligands and halide present. The intervalence Pt(II) $d_{z^2} \rightarrow$ Pt(IV) d_{z^2} charge transfer (CT) band shifts towards lower energy upon compression of the $[M\ldots X–M–X]_n$ chains. An increase in intensity of the CT band possibly reflects the gradual reduction in the inequivalence of the Pt(II) and Pt(IV) coordination environments. However, X-ray diffraction studies of $Pt(C_2H_5NH_3)_4Cl_3{\cdot}2H_2O$ from which the changes in *a*, *b*, and *c* values could be determined showed that the change in the *c* parameter was not sufficient for the Cl group to become equivalent between Pt(II) and Pt(IV). $Pt(C_2H_5NH_3)_4Br_3{\cdot}2H_2O$ is the only complex to show an irreversible transformation to an uncharacterized material (from X-ray powder diffraction data). The same transformation could also be induced by grinding in a pestle and mortar.

Light polarized spectral measurements, parallel to the Pt–Br axis, revealed a red shift of the intervalence, charge-transfer (IVCT) band for the mixed valence complex $[Pt(en)_2][Pt(en)_2Br_2](SO_4)_2{\cdot}6H_2O$ [82] with increasing pressure. A new absorption band appeared above 25 kbar. In the resonance Raman spectrum, the symmetric Pt–Br stretching vibration at 185 cm^{-1} showed a decrease in frequency up to $\sim$30 kbar, but then increased with increasing pressure from 30 to 37 kbar. A new band was observed above 16 kbar, suggesting that the new phase coexists at pressures between 16 and 25 kbar. Initially, $[Pt(en)_2][Pt(en)_2Br_2](SO_4)_2{\cdot}6H_2O$ is transparent to orange light parallel to the chain axis, but as the pressure approached 30 kbar, the sample became dark red and eventually opaque, due to shifts of the charge transfer band towards lower energies. At 40 kbar, the sample appeared to become transparent. This was found to be due to growth of a new phase in which the CT bands and mid-gap bands are at different energies to those of the previous phase. High-resolution Raman measurements demonstrated that both phases coexist throughout the sample over a micrometer scale and that the pressure is uniform. The mechanism of the phase transition was considered.

The Raman-active ν_1 chain modes for the complexes $[Pt(en)_2][Pt(en)_2Cl_2](ClO_4)$ [83] and $Pt(Br)_6(NH_3)_4$ [84] have negative pressure shifts with initial increases in pressure. These shifts are consistent with the template effect and a preferential shortening of the long, weaker Pt(II)–X bonds. For the ethylenediamine complex [83], a continuous shift of the ν_1 Pt–Cl stretch was observed up to 30 kbar, at which pressure a shoulder on the high wavenumber side of the band appeared (Fig. 14). This shoulder steadily gained intensity with further increases in pressure, at the expense of the original band. The original phase was found to coexist with the new high-pressure phase up to at least 60 kbar, the maximum pressure attained. The new high-pressure phase was not identified. The Raman measurements were made on single crystals in the backscattering geometry with respect to the chain axis. For the ammine complex, three pressure domains were observed from ambient pressure to 95 kbar (Fig. 15) [84]. From 1 bar to 30 kbar, ν_1 decreased in frequency. Between 30 and 40 kbar, the slope was essentially zero as each bromide was now at the mid-point between the platinum atoms with these becoming equivalent. At even higher pressures, the sign of the slope changed such that, above 80 kbar, ν_1 exceeded the ambient pressure value. This result could be because at shorter distances there is a repulsion between the Pt and axial Br leading to a bending of the chains to afford a more zigzag structure, at high pressures. A positive shift of the ν_1 mode is observed in 3-D solids, in the absence of a phase transition. A low pressure, quenching of the CDW is observed, and at higher pressures, metallization is obstructed, for example, by either a three-dimensional distortion of the chains or, a transition to another broken symmetry state.

High-pressure absorption, luminescence and Raman spectroscopic studies of Wolframs' red salt, $[Pt(ea)_4][Pt(ea)_2Cl_4](Cl{\cdot}H_2O)_4$ (ea = ethylamine) [85] up to 34 kbar showed a similar response to compression. A rapid decrease of the energy gap below 20 kbar was explained by the increase in the $d(Pt^{IV}–Cl)$ distance as the $d(Pt^{II}–Cl)$ distance decreases with increasing pressures.

A more extensive study of the pressure dependences of the electronic spectra of quasi 1-D semiconductors of the type $K_4[Pt_2(P_2O_5H_2)_4X]\cdot 3H_2O$, X = Cl, Br, ($Pt_2X$, **8**),

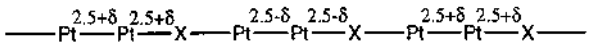

8

has been made by Stroud et al. [86]. The electronic spectrum of these complexes includes bands attributable to the reduced complex $[Bu_4N]_4[Pt_2(P_2O_5H_2)_4]$ (Pt_2), to the oxidized complex $K_4[Pt_2(P_2O_5H_2)_4X_2]\cdot 2H_2O$ (Pt_2Cl_2), and an intense IVCT band. The IVCT band corresponds to $d\sigma^* \rightarrow d\sigma^*$ electron transfer along the chain axis from a Pt_2 dimer to an adjacent Pt_2X_2 dimer (Fig. 16a). For Pt_2Cl, the IVCT band is located at 18 600 cm^{-1}, while in the more delocalized Pt_2Br complex, it is found at lower energy at 16 100 cm^{-1}. As the pressure is increased, the IVCT band shifts to lower energy leveling off at ~ 40 kbar for both Pt_2Cl and Pt_2Br (Fig. 16b). The decrease was of the order of -75 and -100 cm^{-1} $kbar^{-1}$, respectively. These changes are consistent with a continuous change towards a more symmetric

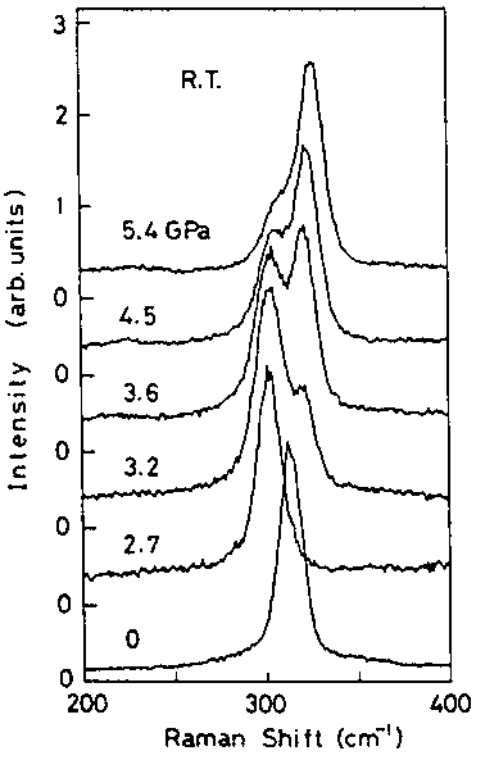

Fig. 14. Raman spectra of the Pt–Cl stretch mode of $[Pt(en)_2][Pt(en)_2Cl_2](ClO_4)_4$ at various pressures. Reprinted with permission from N. Kuroda, M. Sakai, Y. Nishina, K. Sasaki, Phys. Rev. Lett. 68 (1992) 3056. ©1992 American Physical Society.

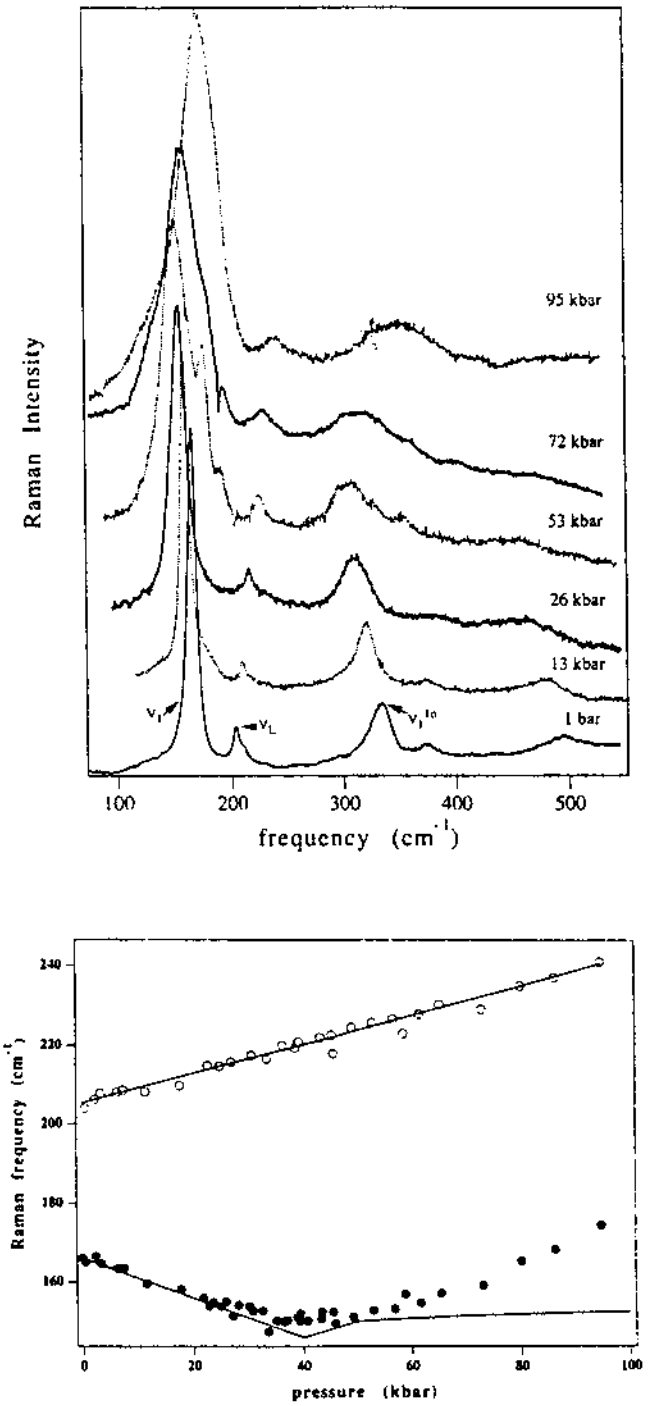

Fig. 15. (a) Raman spectra of $Pt_2Br_6(NH_3)_4$ at various pressures. (b) The pressure dependence at 300 K of the Raman-active chain mode ν_1 (solid circle) and ν_L (hollow circle), the symmetric stretch mode of the equatorial Br ligand in $Pt_2Br_6(NH_3)_4$. Reprinted with permission from G.S. Kanner, J. Tinka Gammel, S.P. Love, S.R. Johnson, B. Scott, B.I. Swanson, Phys. Rev. B 50 (1994) 18682. ©1994 American Physical Society.

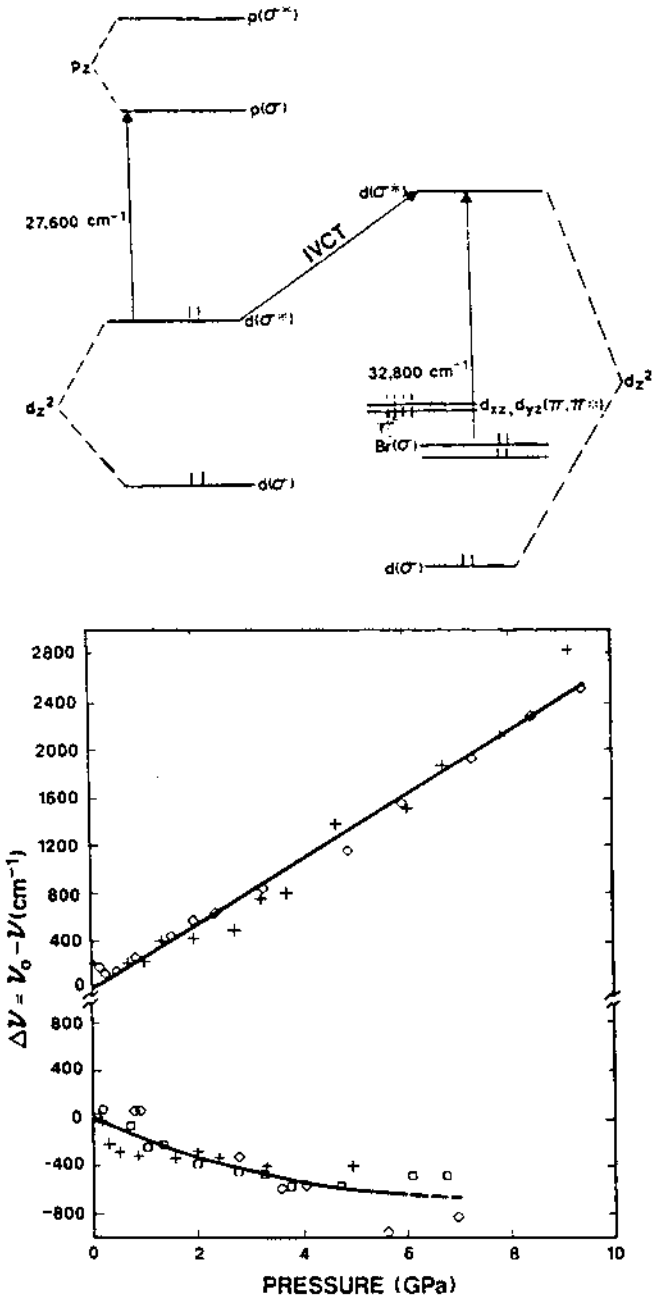

Fig. 16. (a) Energy level diagram for Pt_2Br at ambient pressure. (b) Pressure shift of the $\sigma(Br) \rightarrow d\sigma^*$ transition (top) and the $d\sigma^* \rightarrow p\sigma$ transition (bottom) in Pt_2Br. Reprinted with permission from M.A. Stroud, H.G. Drickamer, M. Heinrichs Zeitlow, H.B. Gray, B.I. Swanson, J. Am. Chem. Soc. 111 (1989) 66. ©1989 American Chemical Society.

structure, with the halogen located equidistant between adjacent Pt_2 dimers, leading to a decrease in the energy difference of $d\sigma^*$ on adjacent Pt_2 dimers. Other spectral changes indicated a destabilization of the $d\sigma^*$ and $p\sigma$ levels through increased orbital overlap and d/p mixing, and a destabilization of the $d_{x^2-y^2}$ level at high pressure through increased ligand field interactions.

The effect of pressure on the $\sigma \rightarrow \sigma^*$ ($\nu_o = 14.7 \times 10^3$ cm^{-1}) and $\pi \rightarrow \sigma^*$ ($\nu_o = 20.8 \times 10^3$ cm^{-1}) metal–metal charge transfer bands in the visible spectrum of $[Pt_2(NH_3)_4(C_5H_5NO)_2]_2(NO_3)_5$ **9**

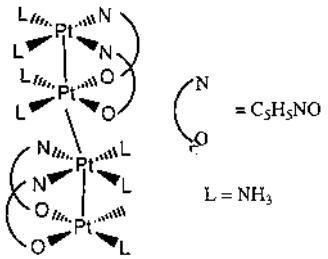

9

dispersed in a polystyrenesulfonic acid medium were measured up to 134 kbar [87]. Other platinum blue tetramers of this type have been synthesized and characterized from which a correlation between the average Pt_4 chain length and the location of the two absorption bands in the visible absorption spectrum was noted, the higher energy band showing a more significant shift with varying chain length. Pressure-tuning of the complex $[Pt_2(NH_3)_4(C_5H_5NO)_2]_2(NO_3)_5$ revealed a dramatic blue-shift of both the bands with increasing pressure: 1690 and 2020 cm^{-1} for the 14.7×10^3 cm^{-1} and 20.8×10^3 cm^{-1} bands, respectively, over 120 kbar (Fig. 17). These results corroborate an electronic model proposed for these complexes and confirm that the change in Pt–Pt distance determines the shift of the absorption bands. A pressure-induced disproportionation, as seen for the tetramer in aqueous media, was observed in the polymeric medium; a significant decrease in the area of the 14.7×10^3 cm^{-1} band and a concomitant increase of the 20.8×10^3 cm^{-1} band with increasing pressure was observed. From calculations, the $\sigma \rightarrow \sigma^*$ (14.7×10^3 cm^{-1}) transition originates from an orbital which involves a net bonding interaction between the inner two platinum atoms and two antibonding interactions between the two sets of outer platinum atoms. The $\pi \rightarrow \sigma^*$ transition (20.8×10^3 cm^{-1}), however, involves excitation from an orbital of two separate weak π interactions between the outer and inner Pt-atoms and an essentially non-bonding interaction between the inner Pt-atoms.

Earlier work on the partially oxidized tetracyanoplatinates, e.g. $K_2[Pt(CN)_4]Br_{0.3}\cdot 3H_2O$, showed increasing conductivity parallel to the chain axis with increasing pressures, and a concomitant decrease in the Pt–Pt distance along the chain [88–90]. Magnus' green salt, $[Pt(NH_3)_4][PtCl_4]$, and related complexes, contain planar $[Pt(NH_3)_4]^{2+}$ and $[PtCl_4]^{2-}$ units which stack in columns in the crystal forming metal chains. The solid-state properties of these materials, e.g. anisotropic conductivity, are due to the direct interaction between the metal atoms.

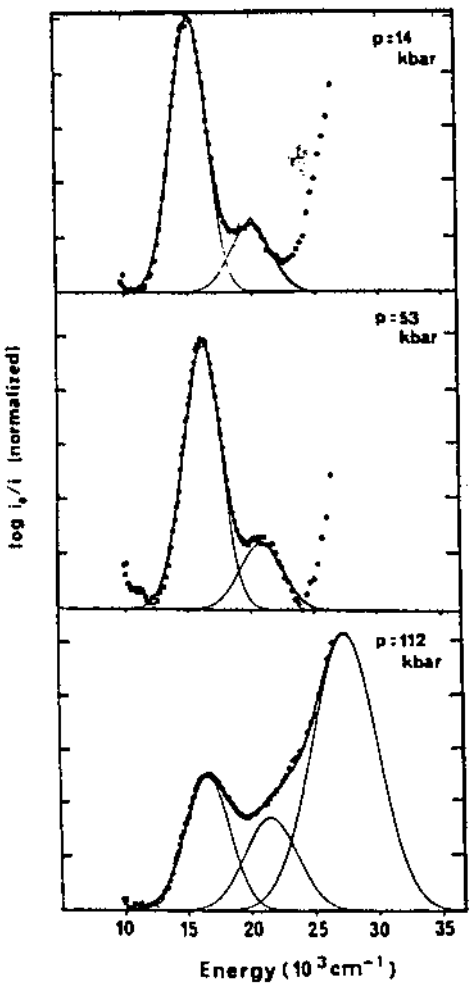

Fig. 17. Visible spectrum of $[Pt_2(NH_3)_4(C_2H_5NO)_2]_2(NO_3)_5$ in PSSA at 14, 53 and 112 kbar. Reprinted from J.L. Coffer, J.R. Shapley, H.G. Drickamer, Chem. Phys. Lett. 149 (1988) 487, with kind permission of Elsevier Science-NL, Sara Burgerhartstraat 25, 1055 KV Amsterdam, The Netherlands.

Electrical, spectral and X-ray diffraction measurements carried out at pressures up to ~ 17 kbar [91] show a continuous change in the lattice parameters and conductivities. The rate of change was dependent on the metal and the initial metal–metal distance in the chain.

There are many complexes which stack to form one-dimensional systems with the associated optical and electrical properties as a direct result of the planar nature of the ligands and the presence of an orbital perpendicular to the plane of the complex, available for bonding. Metal–glyoxime complexes are one such group of complexes. A sharp absorption band observed for crystals of these materials has

been assigned to the optical $n\mathrm{d} \rightarrow (n+1)\mathrm{p}$ interbond transition. This transition is intensified in the crystals by borrowing intensity from a metal-to-ligand charge-transfer excitation. A large red shift of this band, -6×10^{-3} cm^{-1} over 100 kbar, and considerable broadening was observed [92]. This shift was originally ascribed to an electrostatic interaction. A rapid decrease in the electrical resistance of these complexes under pressure, and the red shift of the absorption band, suggested a decreasing band-gap between the filled $n\mathrm{d}_{z^2}$ valence band and $(n=1)\mathrm{p}_z$ conduction band, as the inter-chain metal–metal distance decreased [93]. Resistance minima, as observed for many of the quasi 1-D complexes, are the consequence of a pressure-induced metal $\rightarrow$ ligand electron transfer. High-pressure IR spectroscopy [94] showed a negative pressure shift of one ν(CN) mode, with a second ν(CN) mode disappearing above 17 kbar. A negative pressure shift of the ν(CN) mode indicates an increase in π-backbonding from the metal into a π* orbital of CN. A more recent high-pressure absorption study of Ni, Pd and Pt glyoximes confirmed the shift to lower energy with increasing pressure of the $n\mathrm{d} \rightarrow (n+1)\mathrm{p}$ interband transition [95]. For the Ni and Pd glyoximes, the shift tended to level at higher pressure, but for the Pt complex a reversal of the shift, at sufficiently high pressures, was observed. The initial response to pressure is to further stabilize the excited state, $(n=1)$p, in the order Pt > Pd > Ni, due to the greater spatial extent of orbitals with larger n-values. At sufficiently high pressures the overlap repulsion of the Pt p-orbitals results in the observed blue shift. Intensity borrowing was thought to be the major cause of the dramatic changes in the peak intensities with increasing pressure.

5.6. Other compounds

In the previous section, the pressure-tuning of the charge-transfer bands, or more specifically, the IVCT band, of the quasi one-dimensional platinum complexes and related complexes was discussed. The effect of pressure on the charge transfer band or intervalence-transfer (IT) band, corresponding to an inter-ionic electron transfer has also been studied. Knowledge of the crystal structure of the compounds studied was important in being able to interpret the effect of pressure. A series of 1′,1‴-disubstituted biferrocenium cations with several different substituents and counterions were examined at pressures up to $\sim$150 kbar [96]. The rates of electron transfer varied from relatively valence trapped for complex **10**,

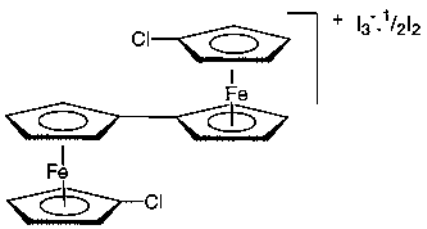

10

to valence detrapped for complex **11**.

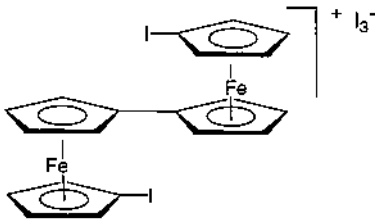

11

The influence of the anion can affect the rate of electron transfer, as can temperature. Complex **12**

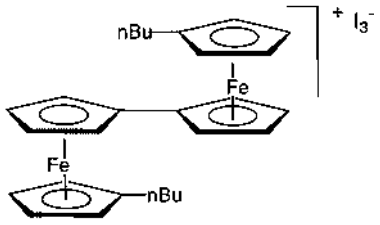

12

becomes valence detrapped at high enough temperatures. Three different types of pressure dependences of the energy of the IT band were seen, which reflected the different arrangement of the anions and cations with respect to one another; (i) alternating anions and cations; (ii) cations located in the interlamellar region of clays and (iii) segregated cation stacks, in which each cation stack is surround by four stacks of anions. An initial blue shift of the IT band for complexes of alternating and intercalated cation structures results from enhanced intermolecular interactions under compression. At high pressures, a red shift of the IT band dominated in the complexes with alternating stacks, due to increased intramolecular interactions (anion/anion and cation/cation) and a reduction in the vibronic coupling in the mixed-valence cation. For the salts with segregated cation stacks, a red shift was observed over the whole pressure range. Similar results were found for the IT bands of the bis(fulvalene)diiron monocation, in various media [crystal lattice, poly(methyl methacrylate) and a zeolite] [97]. The initial blue shift of the charge-transfer bands arose from increased intramolecular interactions and the increase in the energy separation of the bonding ground state and the antibonding excited states of the IT transition with increasing pressure. At higher pressures, but to varying degrees in the different media, intermolecular effects become dominant.

An X-ray crystal structure analysis for $[Cp_2Co]^+I^-$ indicates contact ion pairs. In an attempt to measure the CT bands of the individual ion pairs, electronic absorption spectra were recorded in various polymeric media, viz., poly(methylmethacrylate) (PMMA), polystyrene (PS) and poly(styrenesulfonic acid) (PSSA) [98]. In PMMA and PS, all components of the CT band shifted to lower energies (red shifts). In contrast, blue shifts were observed for all the components in PSSA. PSSA is a highly ionizing polymer, in which $[Cp_2Co]^+I^-$ dissolves as ion pairs, whereas in PMMA and PS, $[Cp_2Co]^+I^-$ is most likely to exist as extensive

aggregates. In the solid state, all the components of the CT band red shifted. The CT band of $[Cp_2Co]PF_6$ is very similar in terms of the number of resolved components and their energies, all the components of the CT of $[Cp_2Co]PF_6$ are blue shifted under compression [99]. In solution, the application of pressure leads to decreased intermolecular and interionic separations, with the resultant increase in charge transfer forces. Such compressional effects are expected to lead to the ground-state stabilization of ionic charge-transfer salts (blue shift). This is observed for such CT salts as *N*-methylacridinium iodide and *N*-methyl-*p*-carbomethoxy-pyridinium iodide, in dichloromethane [98]. In the solid state, neighbouring cation/cation and anion/anion interactions must also be considered, which result in CT destabilization (red shifts). From the crystal structure of $[Cp_2Co]^+I^-$ the distance between the cyclopentadienyl ligands is in fact smaller (3.25 Å) than is the cation-anion interaction of 4.75 Å.

The first three bands of the CT band in $[Cp_2Co]PF_6$ were assigned to three spin-forbidden ligand field transitions, which had become allowed because of the low site symmetry [99]. Further analysis of the band positions and the pressure shifts allowed changes in the ligand field parameters Δ_1 and Δ_2 and the Racah parameter, *B*, to be determined. Pressure-tuning of the electronic levels of Cp_2Fe, $[Cp_2Co]PF_6$ and Cp_2Ni showed that Δ_1 and Δ_2 for these metallocenes changed with pressure in a manner that increases the magnitude of the splitting between the core levels between 2 and 8% for a 100 kbar pressure change [99]. The Racah parameter, *B*, was almost independent of pressure for the metallocenes. These results are consistent with the already very large covalent character of the metallocenes; pressure does not enhance this covalency. On the other hand, compression of ionic compounds increases the d-electron overlap with the ligand orbitals resulting in a greater d-electron shielding and a decreased electron-electron repulsion, leading to changes of the order of 7–15% over 100 kbar in the magnitude of the splitting between the core levels and increases in *B* of 10–15%.

Although not recorded with a DAC, the charge-transfer band of the ion pair, $[Fe(CN)_6]^{4-}\cdot DMV$ (DMV = dimethyl viologen), showed a red shift of ~ 1700 cm^{-1} over 10 kbar pressure [100] in accord with a vibronic coupling model used to describe mixed-valence compounds.

The use of luminescent d^6 transition metal complexes are of current interest as photosensitizers in a number of areas. For luminescent complexes of the general formula *fac*-$[SRe(CO)_3L]^+$, the triplet excited state can be influenced by the ligands, solvent environment, temperature, and pressure effects. The pressure dependences of the emission from some Re(I) complexes, *fac*-$[(py)Re(CO)_3(phen)]$-CF_3SO_3 and *fac*-$[(QPVP)Re(CO)_3(phen)]CF_3SO_3$ [101], and $[Re(phen)_2(py)_2]^+$ and $[Re(phen)_3]^+$ [102] have been investigated. The luminescence characters arise from MLCT [$Re \rightarrow \pi^*$ phen] phosphorescence at room temperature, the excited state being a triplet. The emission peak maximum and its relative intensity for the different Re(I) samples [101] were shown to decrease with increasing pressures up to 70 kbar, the sample dissolved in the polymer PVP (4-vinylpyridine) showing greater pressure sensitivity than did the same complex dissolved in the polymer PAA (poly acrylic acid) (Fig. 18). The increased polarizability of the excited state results in a

decrease in the energy of the transition, the difference in the polarizability of the medium influencing the decrease. Thus, the lower polarizability of the polymer substrate resulted in a reduced pressure sensitivity of the emission. The close correlation between the change in peak energy and intensity with pressure was explained by using the energy gap law, which shows a linear relation between ln K_{nr}, the non-radioactive decay rate constant, and E_{em}, the emission energy. As K_{nr} increases with pressure, I_{em}, the luminescence intensity, will decrease as E_{em} decreases.

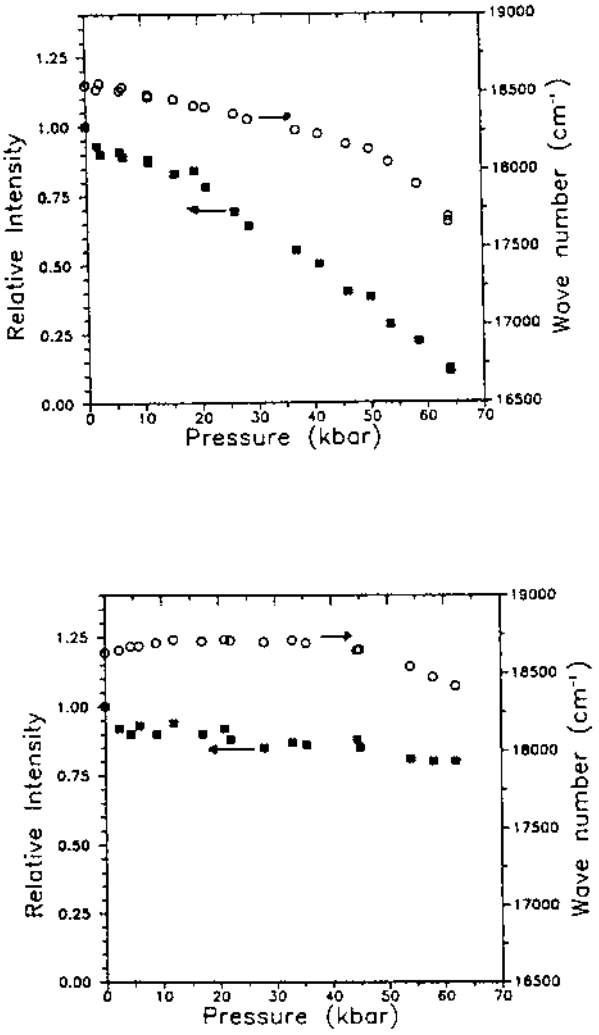

Fig. 18. MLCT emission energy and relative intensity versus pressure for *fac*-[(py)Re(CO)$_3$(phen)]CF$_3$SO$_3$ dissolved in PVP (top) and PAA (bottom). Reprinted with permission form J.M. Lang, Z.A. Dreger, H.G. Drickamer, Chem. Phys. Lett. 192 (1992) 299, with kind permission of Elsevier Science-NL, Sara Burgerhartstraat 25, 1055 KV Amsterdam, The Netherlands.

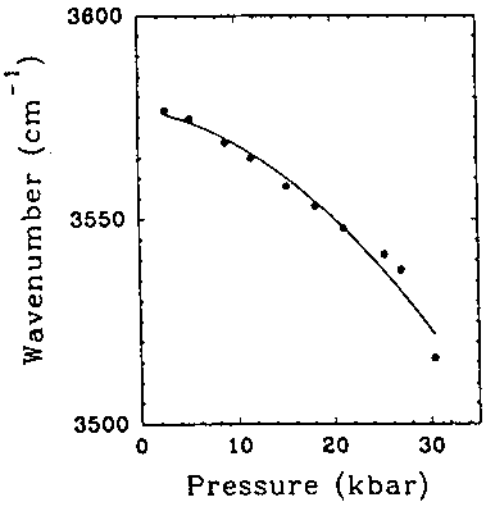

Fig. 19. Pressure dependence of the ν(OH) stretch of the solid HBT-ligand. Reprinted with permission from I.S. Butler, N.T. Kawai, Y. Huang, M. Louloudi, N. Hadjiliadis, Inorg. Chim. Acta 196 (1992) 119.

In the biological field, the complexation of bio-ligands to a metal and subsequent change in the vibrational spectrum have provided important information about the nature of the bonding involved, particularly in biological molecules where several potential ligating sites exist. High-pressure infrared studies up to 30 kbar of a thiamine enzyme intermediate HBT (2-(α-hydroxybenzyl)thiamine chloride) and a mercury(II) complex, $Hg(HBT)Cl_3$ **13**,

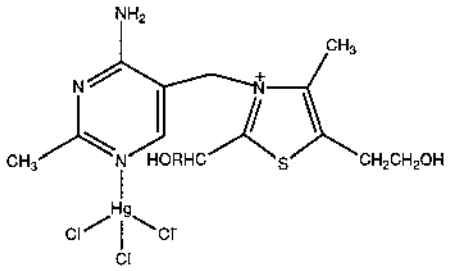

13

revealed that the *S*-conformation of the thiamine enzyme was retained under complexation, its rigidity most likely being due to hydrogen bonding interactions [103]. The ν(OH) mode at 3577 cm^{-1} in the uncomplexed form showed a negative pressure shift, -0.39 cm^{-1} kbar^{-1} (Fig. 19), indicative of increased hydrogen bonding interaction under pressure. The $d\nu/dp$ values for the δC–OH mode of the uncomplexed and complexed form were 0.13 and 0.46 cm^{-1} kbar^{-1}, respectively.

Pressure-tuning IR and solution Raman studies of 17β-estradiol [104] have aided in the assignment of its vibrational spectrum. Furthermore, pressure-tuning studies revealed hydrogen bonding in 17α-ethynyl-estradiol, which is disrupted upon

complexation of an α-[$Cr(CO)_3$] fragment on the arene A-ring. The effects of substitution appeared, however, to be localized to the ring of substitution, most likely because of the rigid nature of the estradiol backbone.

A high-pressure resonance Raman study of the metalloprotein azurin, a blue copper protein, showed that the structure of the protein was essentially independent of pressure up to 36 kbar [105]. The very small shifts of the bands in the 600–100 cm^{-1} region, assigned to the Cu–protein interactions indicated four significant Cu–ligand bonds. Above 36 kbar, a gradual decomposition of the protein occurred, when exposed to laser light. Without exposure to light, the pressure-induced changes were reversible up to 70 kbar.

Pressure-tuning spectroscopy has been widely used in the study of hydrogen-bonding interactions in a large number of organic and ionic compounds. A negative pressure shift of the hydrogenic stretching frequency is observed as weak-medium hydrogen-bonding increases in strength with increasing pressure [106]. A recent high-pressure FT-IR study on Magnus' green salt, $[Pt(NH_3)_4][PtCl_4]$, and two derivatives, $[Pt(ND_3)_4][PtCl_4]$ (MGS-D) and $[Pt(NH_3)_4][PtBr_4]$ (MGS–Br), up to ~40 kbar indicated that weak hydrogen-bonds of the type N–H…Cl do exist in MGS at ambient pressure and that the strength of these hydrogen-bonds increases with increasing pressure [107]. However, it was a negative pressure dependence of the deformation mode, $\delta_s(NH_3)$, observed for all complexes, which indicated the presence of hydrogen-bonding. From X-ray studies, it was unclear as to whether hydrogen-bonding was present or not.

A novel route to the formation of endohedral fullerenes has been proposed which involves insertion of an atom into the vacant cavity of the C_{60} fullerene via formation of a temporary hole within the fullerene cage while the sample is subjected to high temperatures and pressures. This approach has already proved successful for $^3He@C_{60}$, as well as Ne, Ar, Kr and even Xe. To allow insertion of a larger metal atom, however, a larger hole must first be cut in the C_{60} framework. Rubin and co-workers have recently succeeded in producing a 15-membered hole by the consecutive triple scission of a six-member ring on the C_{60} surface via consecutive pericyclic reactions [108]. Subsequent oxidative cobalt insertion affords the Co(III) organometallic complex **14**,

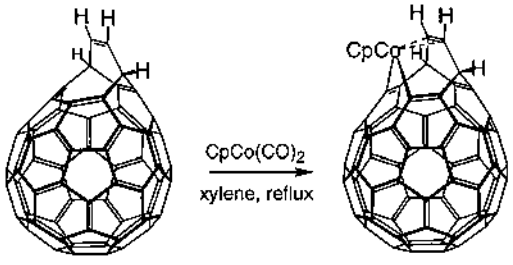

14

$CpCo(C_{64}H_4)$ ($Cp = \eta^5$-C_5H_5), in which an ethylene bridge acts as a η^2-handle to the metal. It was felt that upon application of sufficient external pressures to $CpCo(C_{64}H_4)$, the cobalt atom might be encouraged to slip inside the fullerene cage

through an 11-membered ring. For such an event to occur, the Cp–Co bond would have to be broken. To increase the cobalt–fullerene interaction in $CpCo(C_{64}H_4)$, the strength of the cobalt–ethylene bridge interaction must be increased, via increased π-backbonding from Co to the ethylene bridge. This would result in a negative pressure shift of the ν(C=C) mode. A gradual lengthening of the Cp–Co bond would reveal itself as a gradual shift in the frequency of the ν(Cp–Co) stretching mode to lower wavenumbers with increasing pressure. Both the ν(C=C) mode and the ν(Cp–Co) mode showed distinct positive pressure dependence over the range studied [109]. Pressure-induced insertion was unsuccessful, possibly because of too strong a bond between Co and the Cp ligand. Breaks in the wavenumber versus pressure plots indicate a structural change between 9–13 kbar, most probably due to the rotation of the Cp ligand about the Co–Cp bond, similar to that seen in ferrocene under high pressure [78].

Ring rotation of a different kind was recently identified in the coordination compounds Ph_4M (M = Si, Ge, Sn, Pb) [110]. A phase transition, starting at $\sim$15 kbar, resulted in a curved response, i.e. curved wavenumber versus pressure plots, for many of the observed vibrational modes. The compounds have S_4 symmetry at ambient pressure, with the phenyl rings orientated as in a helicopter propeller. As pressure is applied above 15 kbar, the phenyl rings rotate continuously through all angles, about the P–C bond.

6. Conclusions

Pressure-tuning vibrational and electronic studies have been made on a wide variety of materials; this review has concentrated on a selection of coordination and organometallic compounds that has been studied over the past 15 years. What is perhaps surprising is the lack of theoretical calculations to complement the high-pressure experiments.

Many authors have made extensive use of the X-ray crystal structure data to aid in the interpretation of the pressure-induced shifts of the vibrational and electronic bands. Consideration of the intermolecular spacing, crystal packing and intermolecular interactions, such as π-stacking or hydrogen bonding, can explain many of the observed effects of pressure. For example, the different arrangement of the anions and cations, derived from the crystal structure, was relevant to the observed pressure-induced shifts of the IVCT band of the 1′,1‴-disubstituted biferrocenium salts. Many times, high-pressure X-ray diffraction measurements have provided additional valuable information to aid the interpretation of the spectroscopic data. In the high-pressure study of the one-dimensional complex $Pt(C_2H_5NH_3)_4Cl_3{\cdot}2H_2O$, the change in the lattice parameters under compression confirmed that the red shift of the IVCT band [Pt(II) $d_{z^2} \rightarrow$ Pt(IV) d_{z^2}] was due to a gradual reduction in the inequivalence of the Pt(II) and Pt(IV) coordination environments, but not to the extent that the Cl became equidistant between Pt(II) and Pt(IV).

Some studies have been simply descriptive and proved that one isomer could be transformed into a second under compression, for example, the icosahedral-to-

crown structure transformation of $[Au_9(PPh_3)_8][PF_6]_3$. Each isomer was first prepared synthetically. Other studies have relied upon the literature to provide, for example, ambient pressure electronic energy level diagrams and bonding models. The one-electron energy levels of the Cu(II) ions have been well documented in the literature and have been used extensively in the interpretation of the high-pressure absorption spectra of the many copper complexes studied.

The vast amount of literature concerning metal-carbonyl, metal–thiocarbonyl and metal–alkene coordination was important in the interpretation of the vibrational spectra of these types of compounds under high-pressure. Furthermore, normal coordinate calculations of metal carbonyl and thiocarbonyl compounds made in the late 1970s and early 1980s [111] have provided ambient pressure force constant values, which were taken into account when comparing pressure shifts of the ν(CO) and ν(CS) modes in related compounds. Surprisingly, no reports of force constants under compression have yet been published.

The high-pressure studies on one-dimensional compounds often made extensive use of one-dimensional models proposed in the literature, concerning charge density wave states and Peierls distortions. The MO diagram for Magnus' green salt ($[Pt(NH_3)_4][PtCl_4]$, MGS) was reported by Interrante et al. in 1971 [112], from which the band gap could be determined. The effect of internuclear distance changes on the MGS band structure was calculated and found to corroborate the findings of the effect of pressure on the electronic spectrum well. Sakai and coworkers, made a thorough characterization of the CDW state of $[Pt(en)_2][Pt(en)_2Cl_2](ClO_4)_4$, which allowed the pressure dependences of E_g, β, t_0, the Peierls gap, electron–phonon coupling constant and the super-transfer energy, respectively, and the Peierls distortion, u, of the Cl ions to be clarified from the pressure-induced shifts of optical absorption and Raman scattering spectra. A complete discussion of these calculations has not been included in this review since it represents a more specialized topic.

The use of group theory and correlation tables in determining the nature of a phase transition, whether first or second order, was often demonstrated, particularly by Adams and his coworkers in England.

In the recent literature a molecular dynamics (MD) simulation of pressure-induced crystalline-to-amorphous transitions in corner-linked polyhedral complexes such as quartz, $AlPO_4$ and $LiKSO_4$ were made [113]. Various experimental data from X-ray diffraction, infrared and Raman techniques were available, which indicated the nature of the structural changes prior to and at the phase transition, but a complete microscopic picture at the atomic level was not available. Using a previously described MD method [114], the authors found that the MD simulations provided useful information about the nature of the pathways of the structural changes occurring at high pressures, even though it was carried out on macrocells of only a few hundred atoms.

In conclusion, high-pressure results employing DACs are very encouraging, and it is hoped that in the future, more quantitative results on the influence of high-pressure on materials will start to emerge, whether they be, for example, in the form of force constant calculations or molecular dynamics simulations, for example.

References

[1] R.M. Hazen, The New Alchemists, Times Books, 1993.
[2] M.H. Maghnani, Y. Syono (Eds.), High-Pressure Research: Application to Earth and Planetary Science, Geophys. Monograph 67, Min. Phys., 2, Terra Scientific, Tokyo, 1992.
[3] D.J. Dunstan, in: R. Winter, J. Jonas (Eds.), High-Pressure Chemistry, Biochemistry and Materials Science, 1993, pp. 101–119.
[4] M. Sakashita, H. Yamawaki, K. Aoki, J. Phys. Chem. 100 (1996) 9943.
[5] D.C. Nesting, J.V. Badding, Chem. Mater. 8 (1996) 1535–1539.
[6] J.R. Ferraro, Vibrational Spectroscopy at High External Pressures: The Diamond–Anvil Cell, Wiley, 1984.
[7] (a) H.G. Drickamer, Trends Phys. Chem. 3 (1992) 1. (b) H.G. Drickamer, Annu. Rev. Mater. Sci. 20 (1990) 1. (c) H.G. Drickamer, Chemtracts Anal Phys. Chem. 1 (1989) 271. (d) H.G. Drickamer, Q. Rev. Biophys. 16 (1988) 89. (e) H.G. Drickamer, Acc. Chem. Res. 19 (1986) 329.
[8] S.K. Sherman, A.A. Stadtmuller, Experimental Techniques in High Pressure Research, Wiley, 1987.
[9] D.M. Adams, A.G. Christy, High Temp–High Pressures, 24 (1992) 1.
[10] (a) D.M. Adams, S.J. Payne, K. Martin, Appl. Spec. 27 (1973) 377. (b) D.M. Adams, S.J. Payne, J. Chem. Soc. (1974) 1959.
[11] T.P. Russell, G.J. Piermarini, Rev. Sci. Instrum. 68 (1997) 1835.
[12] M.I.M. Sheerboom, J.A. Schouten, Rev. Sci. Instrum. 67 (1996) 853.
[13] D.J. Dunstan, Rev. Sci. Instrum. 60 (1989) 3789.
[14] For example, H.E. Lorenzana, M. Bennahmias, H. Radousky, Rev. Sci. Instrum. 65 (1994) 3540.
[15] D.D. Ragan, D.R. Clarke, D. Schiferl, Rev. Sci. Instrum. 67 (1996) 494.
[16] (a) D.L. Decker, J. Appl. Phys. 37 (1966) 5012. (b) D.L. Decker, J. Appl. Phys. 42 (1971) 3239.
[17] H.K. Mao, P.M. Bell, J.W. Shaner, D.J. Steinberg, J. Appl. Phys. 49 (1978) 3276.
[18] S.K. Sharma, H.K. Mao, P.M. Bell, J.A. Xu, J. Raman Spectrosc. 16 (1985) 350.
[19] W.F. Sherman, J. Phys. C Solid State Phys. 18 (1985) L973.
[20] R.D. Markwell, I.S. Butler, Can. J. Chem. 73 (1995) 1019.
[21] K.L. Baldwin, S. Webster, D.N. Batchelder, in: S.A. Asher, P.B. Stein (Eds.), Proceedings of the XVth International Conference on Raman Spectroscopy, Pittsburgh, 1996, pp. 1162–1163.
[22] I.S. Butler, C.M. Edwards, R.D. Markwell, Spectrochim. Acta 53A (1997) 2253.
[23] D.D. Klug, E. Whally, Rev. Sci. Instrum. 54 (1983) 1205.
[24] See for example, W.F. Sherman, G.R. Wilkinson, in: R.J.H. Clark, R.E. Hester (Eds.), Advances in Infrared and Raman Spectroscopy, vol. 6, Heydon and Son, London, 1980.
[25] (a) D.M. Adams, I.O.C. Ekejiuba, J. Chem. Phys. 77 (1982) 4793. (b) D.M. Adams, L.M. Davey, P.D. Hatton, A.C. Shaw, J. Mol. Struc. 79 (1982) 415.
[26] Y. Huang, I.S. Butler, D.F.R. Gilson, Spectrochim. Acta 47A (1991) 909.
[27] Y. Huang, I.S. Butler, D.F.R. Gilson, D. Lafleur, Inorg. Chem. 30 (1991) 117.
[28] D.M. Adams, P.W. Ruff, D.R. Russell, J. Chem. Soc. Faraday Trans. 87 (1991) 1831.
[29] (a) M.A. Andrews, J. Eckert, J.A. Goldstone, L. Passell, B. Swanson, J. Am. Chem. Soc. 105 (1983) 2262. (b) D. Lafleur, MSc thesis, McGill University, 1988.
[30] G.P. McQuillan, D.C. McKean, C. Long, A.R. Morrison, I. Torto, J. Am. Chem. Soc. 108 (1986) 863.
[31] (a) D.M. Adams, P.D. Hatton, A.C. Shaw and T.-K. Tan, J. Chem. Soc. Chem. Comm. (1981) 226. (b) D.M. Adams, P.D. Hatton, A.C. Shaw, J. Phys. Condens. Matter 3 (1991) 6145.
[32] D.M. Adams, I.O.C. Ekejiuba, J. Chem. Phys. 78 (1983) 5408.
[33] Y. Huang, I.S. Butler, D.F.R. Gilson, Inorg. Chem. 30 (1991) 1098.
[34] Y. Huang, I.S. Butler, D.F.R. Gilson, Inorg. Chem. 31 (1992) 4762.
[35] D.L. Lichtenberger, R.F. Fenske, Inorg. Chem. 15 (1976) 2015.
[36] Y. Huang, I.S. Butler, D.F.R. Gilson, Inorg. Chem. 31 (1992) 303.
[37] D. Lesage, Honors Project Research Report, McGill University, 1994.
[38] C.M. Edwards, Ph.D. Thesis, McGill University, 1998.
[39] M. Minelli, W.J. Maley, Inorg. Chem. 28 (1989) 2954.

[40] H. Li, I.S. Butler, Inorg. Chem. 34 (1995) 1193.
[41] D.M. Adams, P.A. Fletcher, Spectrochim. Acta 44A (1988) 437.
[42] J.A. Baldwin, I.S. Butler, D.F.R. Gilson, Spectrochim. Acta, submitted for publication.
[43] J.L. Coffer, J.R. Shapley, H.G. Drickamer, Inorg. Chem. 29 (1990) 3900.
[44] K.L. Bray, H.G. Drickamer, D. Michael, P. Mingos, M.J. Watson, J.R. Shapley, Inorg. Chem. 30 (1991) 864.
[45] H.G Drickamer, K.L. Bray, Acc. Chem. Res. 23 (1990) 55.
[46] K.L. Bray, H.G. Drickamer, E.A. Schmitt, D.N. Hendrickson, J. Am. Chem. Soc. 111 (1989) 2849.
[47] K.L. Bray, H.G. Drickamer, J. Phys. Chem. 93 (1989) 7604.
[48] K.L. Bray, H.G. Drickamer, J. Phys. Chem. 95 (1991) 559.
[49] K.L. Bray, H.G. Drickamer, J. Phys. Chem. 94 (1990) 2154.
[50] For example (a) G.L. Kubas, C.J. Unkefer, B.I. Swanson and E. Fukushima, J. Am. Chem. Soc. 108 (1986) 7000. (b) L. Wisniewski, M. Mediati, C.M. Jensen, K.W. Zilm, J. Am. Chem. Soc. 115 (1993) 7533.
[51] R.D. Markwell, I.S. Butler, C.M. Edwards, C. Bianchini, M. Peruzzini, D. Burns, A. Fafara, J. Chem. Soc. Chem. Commun., submitted for publication.
[52] C.M. Edwards, Ph.D. Thesis, McGill University, 1998.
[53] See for example (a) G.J. Kubas, R.R. Ryan, B.I. Swanson, P.J. Vergamini, H.J. Wasserman, J. Am. Chem. Soc. 106 (1984) 451. (b) G.J. Kubas, C.J. Burns, J, Eckert, S.W. Johnson, A.C. Larson, P.J. Vergamini, C.J. Unkefer, G.R.K. Khalsa, S.A. Jackson, O. Eisenstein, J. Am. Chem. Soc. 115 (1995) 569.
[54] See for example (a) D. Michos, X.L. Luo, J.A.K. Howard, R.H. Crabtree, Inorg. Chem. 31 (1992) 3194. (b) F.A. Cotton, R.L. Luck, Inorg. Chem. 30 (1991) 767.
[55] C.M. Edwards, Ph.D. Thesis, McGill University, 1998.
[56] T.L. Carroll, J.R. Shapley, H.G. Drickamer, J. Am. Chem. Soc. 107 (1985) 5802.
[57] T.L. Carroll, J.R. Shapley, H.G. Drickamer, J. Chem. Phys. 85 (1986) 6787.
[58] J.R. Shapley, H.G. Drickamer, J. Clus. Sci. 5 (1994) 145.
[59] (a) D.E. Morris, C.D. Tait, R.B. Dyer, J.R. Schoonover, M.D. Hopkins, A.P. Sattelberger, W.H. Woodruff, Inorg. Chem. 29 (1990) 3447. (b) D.E. Morris, A.P. Sattelberger, W.H. Woodruff, J. Am. Chem. Soc. 108 (1986) 8270.
[60] T.L. Carroll, J.R. Shapley, H.G. Drickamer, Chem. Phys. Lett. 119 (1985) 340.
[61] R.T. Roginski, T.L. Carroll, A. Moroz, B.R. Whittlesey, J.R. Shapley, H.G. Drickamer, Inorg. Chem. 27 (1988) 3701.
[62] (a) F.A. Cotton, D.G. Lay, Inorg. Chem. 20 (1981) 935. (b) G.S. Girolami, R.A. Andersen, Inorg Chem. 21 (1982) 1318.
[63] See Refs. [11–14, 18, 20–22] in Ref. 58(a).
[64] J.L. Coffer, H.G. Drickamer, J.T. Park, R.T. Roginski, J.R. Shapley, J. Phys. Chem. 94 (1990) 1981.
[65] J.L. Coffer, H.G. Drickamer, J.R. Shapley, J. Phys. Chem. 94 (1990) 5208.
[66] R. Chevrel, M. Hirrien, M. Sergent, Polyhedron 5 (1986) 87.
[67] J.L. Coffer, J.R. Shapley, H.G. Drickamer, Polyhedron 8 (1989) 801.
[68] D.M. Adams, M. Pogson, J. Phys. C: Solid State Phys. 21 (1988) 1065.
[69] J.J. Rush, W.C. Hamilton, Inorg. Chem. 5 (1996) 2238.
[70] (a) L.A. de Graaf , Chr. Steenbergen, Physica, 97B (1979) 199. (b) ibid 94B (1978) 228. (c) Chr. Steenbergen, J.J. Rush, J. Chem. Phys. 70 (1979) 50. (d) H. den Adel, H.B. Brom, D.J. Ligthelm, R.A. Wind, Physica 111B (1981) 171.
[71] D.M. Adams, J. Haines, J. Chem. Soc. Faraday Trans. 88 (1992) 3587.
[72] D.M. Adams, J. Haines, Spectrochim. Acta 49A (1993) 237.
[73] M. Pagannone, H.G. Drickamer, J. Chem. Phys. 43 (1965) 4064.
[74] J. Eckert, R. Youngblood, Solid State Comm. 44 (1982) 1393.
[75] D.M. Adams, S.J. Payne, Inorg. Chim. Acta 19 (1976) L49.
[76] D.M. Adams, J. Haines, J. Phys Chem. 95 (1991) 7068.

[77] (a) I.J. Hyaus, A. Ron, J. Chem. Phys. 59 (1973) 3027. (b) I.J. Hyaus, J. Chem. Phys. Lett. 18 (1973) 399.
[78] D.M. Adams, A.D. Williams, J. Phys. Chem. Solids 41 (1980) 1073.
[79] R.T. Roginski, A. Moroz, H.G. Drickamer, Chem. Phys. Lett. 143 (1988) 577.
[80] R.T Roginski, J.R. Shapley, H.G. Drickamer, J. Phys. Chem. 92 (1988) 4316.
[81] L.V. Interrante, K.W. Browall, F.P. Bundy, Inorg. Chem. 13 (1974) 1158.
[82] N. Matsushita, N. Kuroda, Mol. Cryst. Liq. Cryst. 256 (1994) 867.
[83] N. Kuroda, M. Sakai, Y. Nishina, K. Susaki, Phys. Rev. Lett. 68 (1992) 3056.
[84] G.S. Kanner, J.T. Gammel, S.P. Love, S.R. Johnson, B. Scott, B.I. Swanson, Phys. Rev. B 50 (1994) 18682.
[85] H. Tanino, N. Koshizuka, K. Kobayashi, M. Yamashita, K. Hoh, J. Phys. Soc. Jpn. 54 (1985) 483.
[86] M.A. Stroud, H.G. Drickamer, M. Heinrichs Zeitlow, H.B. Gray, B.I. Swanson, J. Am. Chem. Soc. 111 (1989) 66.
[87] J.L. Coffer, J.R. Shapley, H.G. Drickamer, Chem. Phys. Lett. 149 (1988) 487.
[88] B. Renker, L. Bernard, C. Vettier, R. Comes, B.P. Schweiss, Solid State Commun. 41 (1982) 935.
[89] H. Kobayashi, A. Kobayashi, K. Asaumi, S. Minonura, Solid State Commun. 35 (1980) 293.
[90] Y. Hara, I. Shirotani, A. Onodera, Solid State Commun. 17 (1975) 827.
[91] L.V. Interrante, F.P. Bundy, Inorg. Chem. 10 (1971) 1169.
[92] J.C. Zahner, H.G. Drickamer, J. Chem. Phys. 33 (1990) 1625.
[93] Y. Hara, I. Shirotani, A. Onodera, Solid State Commun. 19 (1976) 171.
[94] Y. Hara, M.F. Nicol, Bull. Chem. Soc. Jpn. 51 (1978) 1982.
[95] M. Tkacz, H.G. Drickamer, J. Chem. Phys. 85 (1986) 1184.
[96] U. Sinha, M.D. Lowery, W.W. Ley, H.G. Drickamer, D.N. Hendrickson, J. Am. Chem. Soc. 110 (1988) 2471.
[97] U. Sinha, M.D. Lowery, W.S. Hammack, D.N. Hendrickson, H.G. Drickamer, J. Am. Chem. Soc. 109 (1987) 7340.
[98] T.M. Bockman, H.R. Chang, H.G. Drickamer, J.K. Kochi, J. Phys. Chem. 94 (1990) 8483.
[99] R.T. Roginski, A. Moroz, D.N. Hendrickson, H.G. Drickamer, J. Phys. Chem. 92 (1988) 4319.
[100] W.S. Hammack, H.G. Drickamer, D.N. Hendrickson, Chem. Phys. Lett. 151 (1988) 469.
[101] J.M. Lang, Z.A. Dreger, H.G. Drickamer, Chem. Phys. Lett. 192 (1992) 299.
[102] J.M. Lang, Z.A. Dreger, H.G. Drickamer, J. Phys. Chem. 97 (1993) 2289.
[103] I.S. Butler, N.T. Kawai, Y. Huang, M. Louloudi, N. Hadjiliadis, Inorg. Chim. Acta 196 (1992) 119.
[104] S.M. Barnet, I.S. Butler, S. Top, G. Jaouen, Vib. Spectrosc. 8 (1995) 263.
[105] S.F. Agnew, J.R. Schoonover, B.I. Swanson, W.H. Woodruff, J. Am. Chem. Soc. 107 (1985) 6716.
[106] See S.D. Hamann, Aust. J. Chem. 32 (1978) 11, and references therein.
[107] C.M. Edwards, I.S. Butler, unpublished results.
[108] M.J. Arce, A.L. Viado, Y.-Z. An, S.I. Khan, Y. Rubin, J. Am. Chem. Soc. 118 (1996) 3775.
[109] C.M. Edwards, I.S. Butler, W. Qian, Y. Rubin, J. Mol. Struct. 442 (1998) 169.
[110] S.D. Warner, I.S. Butler, I. Wharf, Coord. Chem. Rev. (1998) submitted.
[111] See for example (a) G.P. McQuillan, D.C. McKean, C. Long, A.R. Morrisson, I. Torto, J. Am. Chem. Soc. 108 (1986) 863. (b) A.M. English, K.R. Plowman, I.S. Butler, Inorg. Chem. 21 (1982) 338. (c) A.M. English, K.R. Plowman, I.S. Butler, Inorg. Chem. 20 (1981) 2553. (d) I.S. Butler, A. Garcia-Rodriguez, K.R. Plowman, C.F. Shaw III, Inorg. Chem. 15 (1976) 2602.
[112] L.V. Interrante, R.P. Messmer, Inorg. Chem. 10 (1971) 1174.
[113] S.L. Chaplot, S.K. Sikka, Phys. Rev. B 47 (1993) 5710.
[114] S.L. Chaplot, Curr. Sci. 55 (1986) 949.